



One way of representing the size and shape of biomass particles in combustion modeling

Title	One way of representing the size and shape of biomass particles in combustion modeling
Author(s)	Trubetskaya, Anna;Beckmann, Gert;Wadenbäck, Johan;Holm, Jens Kai;Velaga, Sitaram P.;Weber, Roman
Publication Date	2017-06-29
Publisher	Elsevier
Repository DOI	10.1016/j.fuel.2017.06.052

1
2
3
4
5
6
7
8
9 One way of representing the size and shape of biomass
10 particles in combustion modeling
11
12
13

14 Anna Trubetskaya^{a,*}, Gert Beckmann^b, Johan Wadenbäck^c, Jens Kai
15 Holm^d, Sitaram P Velaga^e, Roman Weber^f
16

17 ^a*Division of Energy Science, Luleå University of Technology, 97187 Luleå, Sweden*

18 ^b*Retsch GmbH, Retsch Allee 15, 42781 Haan, Germany*

19 ^c*Amager power plant, HOFOR A/S, Kraftværkvej 37, 2300 Copenhagen S, Denmark*

20 ^d*DONG Energy Thermal Power A/S, Nesa Alle 1, 2820 Gentofte, Denmark*

21 ^e*Department of Health Sciences, Luleå University of Technology, 97187 Luleå, Sweden*

22 ^f*Institute of Energy Processes Engineering and Fuel Technology, Clausthal University of
23 Technology, 38678 Clausthal-Zellerfeld, Germany*
24
25
26
27

28
29 **Abstract**
30
31

32 This study aims to provide a geometrical description of biomass particles that
33 can be used in combustion models. The particle size of wood and herbaceous
34 biomass was compared using light microscope, 2D dynamic imaging, laser
35 diffraction, sieve analysis and focused beam reflectance measurement. The
36 results from light microscope and 2D dynamic imaging analysis were com-
37 pared and it showed that the data on particle width, measured by these two
38 techniques, were identical. Indeed, 2D dynamic imaging was found to be the
39 most convenient particle characterization method, providing information on
40 both the shape and the external surface area. Importantly, a way to quantify
41 all three dimensions of biomass particles has been established. It was recom-
42 mended to represent a biomass particle in combustion models as an infinite
43 cylinder with the volume-to-surface ratio (V/A) measured using 2D dynamic
44
45
46
47
48
49
50
51
52
53
54
55

56 ^{*}Corresponding author. anna.trubetskaya@ltu.se
57
58

1
2
3
4
5
6
7
8
9 imaging.

10
11 *Keywords:* biomass, 2D dynamic imaging, FBRM, laser diffraction, sieving
12
13

14
15 **Nomenclature**
16

17			
18	A	Particle surface area [m ²]	Q_3 Cumulative particle distribu-
19			tion, based on volume [%]
20			
21	AR	Aspect ratio	
22			
23			\bar{q}_3 Histogram
24	b	Particle width [m]	
25			
26			q_3 Frequency particle distribu-
27	c_p	Specific heat capacity [J (kg	tion, based on volume [%
28		K) ⁻¹]	mm ⁻¹]
29			
30			
31			
32	d	Diameter [m]	r Particle radius [m]
33			
34			
35	f	Dimensionality factor	r_1, r_2 Distances from the area center
36			to the particle edges [m]
37	l	Particle length [m]	
38			
39			
40	L	Chord length [m]	$SPHT$ Circularity (Sphericity)
41			
42			
43	m	Number of size classes	$Symm$ Symmetry
44			
45			
46	M_i	Class midpoint [m]	T Temperature [°C]
47			
48			
49	N	Class number	t Time [s]
50			
51			
52	n	Number of counts per size class	V Volume [m ³]
53			
54			
55	P	Perimeter of a particle projec-	w Size class weight
56		tion [m]	x_{cmin} Smallest maximal chord [m]
57			
58			

1
2
3
4
5
6
7
8
9
10
11
12
13
14
15
16
17
18
19
20
21
22
23
24
25
26
27
28
29
30
31
32
33
34
35
36
37
38
39
40
41
42
43
44
45
46
47
48
49
50
51
52
53
54
55
56
57
58
59
60
61
62
63
64
65

x_{Feret} Feret maximum diameter [m] ρ Density [kg m⁻³]

x_{Martin} Martin minimum diameter [m] **Subscripts**

e Effective

Greek symbols

p Particle

λ Thermal conductivity [W (m K)⁻¹]

s Solid phase

$total$ Total

1. Introduction

Biomass firing is used for power generation and is considered an important step in the reduction of greenhouse gas emissions. Anthropogenic CO₂ emissions can be decreased by biomass co-firing due to the lower regeneration time of biomass compared to bituminous coal. Thus, CO₂ released with biofuels can be reconsumed faster by plants via photosynthesis than the time needed to regenerate coal. The milling process is a necessary step in suspension firing [1]. Size reduction improves fuel conversion processes because of the creation of larger reactive surface areas [2, 3]. Biomass is, due to its fibrous structure, difficult to mill. Since the heating value of biomass is lower than coal, more biomass has to be used in order to achieve the same power output [4, 5]. Increased energy input into biomass comminution affects the total efficiency of a power plant, and too large particles often cause problems with flame stability and burnout.

Fuel characterization plays an important role in combustion modeling [6–11]. The surface area and volume of the particle are important parameters

1
2
3
4
5
6
7
8
9
10 since they determine combustion rates and define residence time. Various
11 biomass shapes result in different volume-to-surface area ratios, which are
12 important parameters in describing heat and mass transfer processes. For a
13 given volume, spheres represent the largest volume-to-surface area ratio of
14 any shape, which makes an assumption of spherical particles in combustion
15 modeling rather conservative. Particle size analysis methods that assume
16 a constant (spherical) shape are inadequate for biomass since irregularly
17 shaped particles are typical and most often present. Furthermore, a dis-
18 agreement between particle size distributions obtained by many particle size
19 measurement techniques has been observed [12]. Most particle analyzers use
20 one geometrical parameter by assuming a spherical form. However, as the
21 fuel particle shape becomes more complex, at least two parameters (width
22 and length) are necessary to describe the particle size.

23
24
25
26
27
28
29 Despite numerous studies on biomass particles [7, 9–11, 13, 14], there is
30 no consensus on how to represent a biomass particle in combustion models.
31 The common way involves approximating of the particle shape to regular ge-
32 ometrical bodies (e.g. parallelepiped, cylinder, cubes, ellipsoids). In combus-
33 tion models from Yang et al. [14] and Yin et al. [13], particles are represented
34 by cylindrical and spherical shapes, whereas Thunman et al. [7] treat parti-
35 cles in a one-dimensional model as plates, cylinders and spheres representing
36 non-spherical shapes. The accuracy of particle models depends on both cor-
37 rect size distribution and characterization of fuel inhomogeneity in terms of
38 shape and structure. The objective of this study is twofold: (1) to provide a
39 geometrical description of biomass particles that can be used in combustion
40 model; (2) to make suggestions for the size and shape of biomass particles.

1
2
3
4
5
6
7
8
9
41 In this work, the biomass particles' size and shape are characterized by using
10 both 2D dynamic imaging analysis and microscopy. 2D dynamic imaging
11 results are compared with particle size data obtained using focused beam
12 reflectance measurement, laser diffraction and sieving techniques.
13
14
15
16
17

18 2. Materials and methods

19 2.1. Raw material characterization

20
21
22
23 Table 1 lists samples which were used in the particle size and shape
24 characterization study.
25
26
27

28 Table 1: Samples specification. The bulk density, ash (% dry basis) and moisture (%
29 as received) content were determined for poplar, wheat straw and pulverized wood
30 pellets. Samples were comminuted in the rotor- and Loesche roller mills. Prior to
31 particle size and shape analysis, samples were collected using a rotorprobe and a
32 micro-riffler.
33
34
35
36
37

Identifier	Samples		
	Poplar	Pulverized wood pellets	Wheat straw
mill type	Rotor mill	Loesche roller mill	Rotor mill
sampling method	Micro-riffler	Rotorprobe	Micro-riffler
bulk density, g cm ⁻³	1.4	1.3	1.4
ash, % dry basis	1.3	0.5	4.1
moisture, % as received	7.9	7.8	10

38
39
40
41
42
43
44
45
46
47
48
49
50
51
52
53
54
55
56
57
58
59
60
61
62
63
64
65

49 Wheat straw and wood pellets represent the fuel types which are com-
50 monly used for suspension fired combustion with 100% biomass. It is a
51 challenge to obtain high operational flexibility at power plants by applica-
52 tion of a broad biofuel range. Therefore, poplar, which is among the fastest

1
2
3
4
5
6
7
8
9
10 53 growing trees in the world, was selected for this study [15]. The moisture
11 54 content and bulk density were measured using standard methods described
12
13 55 in EN ISO 18134-1:2015 and EN ISO 17828:2015. The ash content was de-
14
15 56 termined using a standard ash test at 550°C, according to the procedure
16
17 57 described in EN ISO 18122:2015. The 8 mm pellets, without additives or
18
19 58 binding agents, were produced in Latvia (LatGran). The pellets were trans-
20
21 59 ported to Avedøre power plant and comminuted in the horizontal Loesche
22
23 60 roller mill. Pulverized wood was sampled from the pipeline (running to the
24
25 61 burners) through a side opening by using a rotorprobe. Pellets consisted
26
27 62 of 10 % hardwood and 90 % softwood, and were produced from 70 % fine
28
29 63 sawdust and 30 % coarse sawdust. A larger percentage of softwood contains
30
31 64 Scots pine (*Pinus sylvestris*), Norway spruce (*Picea abies*) and European as-
32
33 65 pen (*Populus tremula*), whereas a smaller percentage of hardwood consists
34
35 66 of birch (*Betula* spp) and alder (*Alnus* spp), according to the feedstock clas-
36
37 67 sification described in EN ISO 17225-1. The age of the roundwood with bark
38
39 68 used for making pellets ranged from 15 to 95 years.

40 69 Poplar and wheat straw samples were milled in a ZM200 rotor mill
41
42 70 (Retsch GmbH, Germany) whereas pellets were comminuted in a LM 23.2 D
43
44 71 horizontal roller mill (Loesche GmbH, Germany). All samples were milled
45
46 72 to < 0.5 mm. Biomass samples were sieved to the 0.71-1 mm particle size
47
48 73 fraction. Under fast heating conditions, which are relevant to suspension
49
50 74 firing, biomass particles with mean diameters < 0.425 mm may be consid-
51
52 75 ered as thermally thin based on the previous modeling results [16], while the
53
54 76 intra-particle heat conduction in larger particles plays a key role in biomass
55
56 77 devolatilization. The previous results also indicated that the larger wood

1
2
3
4
5
6
7
8
9 78 particles (0.85-1 mm) required more than 1 s in the wire-mesh and drop tube
10 79 reactors at 1000°C for complete conversion [17]. Therefore, the large biomass
11 80 particles were selected for the shape characterization study because particles
12 81 of size > 0.7 mm can often cause problems with flame stability and burnout.
13 82 Prior to the analysis, biomass samples were divided into equal (100 mg) frac-
14 83 tions using a PT100 micro-riffler (Retsch GmbH, Germany).

21 84 *2.2. Particle size and shape characterization*

22 85 *2D dynamic imaging analysis.* The particle size and shape were measured
23 86 using the CAMSIZER (Retsch GmbH, Germany), designed for the particle
24 87 size range from 0.03 to 30 mm. Particle shadows (projected area) were cap-
25 88 tured by two cameras: a zoom camera, designed for the analysis of smaller
26 89 particles, and a basic-camera that was able to detect larger particles. The
27 90 particle projected area was determined using the CAMSIZER 6.3.10 soft-
28 91 ware (Retsch GmbH, Germany) which evaluates the particle size from the
29 92 captured images by calculating the three parameters shown in Figure 1.

1
2
3
4
5
6
7
8
9
10
11
12
13
14
15
16
17
18
19
20
21
22
23
24
25
26
27
28
29
30
31
32
33
34
35
36
37
38
39
40
41
42
43
44
45
46
47
48
49
50
51
52
53
54
55
56
57
58
59
60
61
62
63
64
65

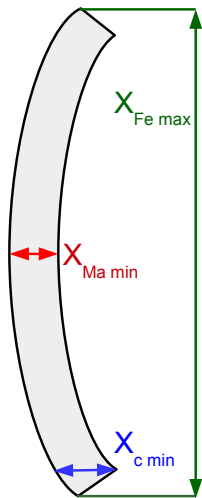


Figure 1: Martin minimal ($x_{Ma\ min}$), smallest maximal chord ($x_{c\ min}$) and Feret maximal ($x_{Fe\ max}$) diameters for a particle projection, as also shown in the Supplemental material.

93 The smallest maximal chord ($x_{c\ min}$) is defined as the smallest of all maximum
94 chords of a particle projection. The Martin diameter is a characteristic
95 length that divides the projected particle area into two equal halves [18]. The
96 minimal Martin diameter ($x_{Ma\ min}$) is determined from the smallest Martin
97 diameter of a particle projection [19]. The Feret diameter is a distance between
98 two tangents placed perpendicular to the measurement direction [18].
99 The Feret maximal diameter is the longest Feret diameter of all measured
100 Feret diameters of a particle projection [19]. The particle size distribution,
101 based on the volume as shown in the Supplemental material, is represented
102 by the $x_{Ma\ min}$ diameter. For the particle size analysis, a 100 mg sample was

1
2
3
4
5
6
7
8
9
103 used.

104 *Shape characterization.* In the present study, particle shape is characterized
105 by both the sphericity (SPHT) and the aspect ratio (AR). Sphericity is one
106 of the most commonly used parameters to express the deviation of a two-
107 dimensional particle image from a sphere / circle and is defined as

$$SPHT = \frac{4 * \pi * A}{P^2}, \quad (1)$$

108 where P and A are the measured perimeter and area of a particle projection,
109 respectively. A particle is considered to be spherical when sphericity is equal
110 to 1, and non-spherical when it is less than 1. The aspect ratio is defined as
111 the ratio of particle width ($b = x_{M_{amin}}$) to the particle length ($l = x_{F_{emax}}$)
112 so that

$$AR = \frac{b}{l}. \quad (2)$$

113 Particle symmetry (Symm) is defined as

$$Symm = \frac{1}{2} \left(1 + \left(\min \frac{r_1}{r_2} \right) \right), \quad (3)$$

114 where r_1 and r_2 are distances from the area center to the particle edges
115 on the same line. The center (C) of area in Figure 2 is determined by the
116 CAMSIZER software. Many lines are drawn so that each one passes through
117 the area center between the particle's edges. The symmetry is calculated
118 from the smallest ratio of the resulting segments (r_1 and r_2). For highly
119 symmetrical particles like circles, ellipses or squares, the symmetry nears
120 one. The center point divides each line in two parts. For asymmetrical
121 particles (e.g. broken beads, triangles), the symmetry is less than one. The

1
2
3
4
5
6
7
8
9
122 symmetry varies from 0 to 0.5, and r_1 and r_2 overlap, if the center of the area
123 is outside of a particle so that

$$\frac{r_1}{r_2} < 0. \quad (4)$$

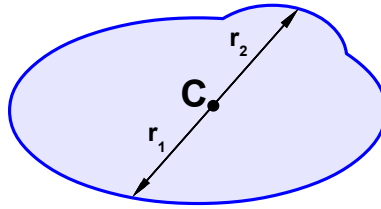


Figure 2: Definition of symmetry.

124 The symmetry is equal to 0.5, if the center of the area is exactly at the
125 particle border.

126 *Sieving.* A vibrating AS 200 sieve shaker (Retsch GmbH, Germany) compris-
127 ing seven sieves ranging from 0.25 to 4 mm in opening size and a bottom pan
128 (< 0.25 mm) was used. The sieving analysis is described in EN ISO 17827-
129 2:2016. Particles remaining on each sieve and in a bottom pan were collected
130 and weighed using an electronic top pan balance (± 0.01 g accuracy). The
131 cumulative retained undersize is the mass passed from the previous sieve,
132 minus the mass retained on the current sieve [20]. Sieving was conducted for
133 15 min at 3 mm amplitude [21].

134 *Particle size distribution.* The results are presented as a cumulative parti-
135 cle size distribution, based on volume (Q_3). The cumulative particle size

1
2
3
4
5
6
7
8
9
10
11
12
13
14
15
16
17
18
19
20
21
22
23
24
25
26
27
28
29
30
31
32
33
34
35
36
37
38
39
40
41
42
43
44
45
46
47
48
49
50
51
52
53
54
55
56
57
58
59
60
61
62
63
64
65

136 distribution is described in EN ISO 9276-1:1998, and is defined as

$$Q_3(x_{M a m i n, m}) = \sum_{i=1}^m \bar{q}_3(x_{M a m i n, i}) \Delta x_{M a m i n, i}, \quad (5)$$

137 where \bar{q}_3 is the area of the histogram. The results of a particle size analysis
138 are also presented as a frequency distribution over $x_{M a m i n}$, based on volume
139 (q_3), so that

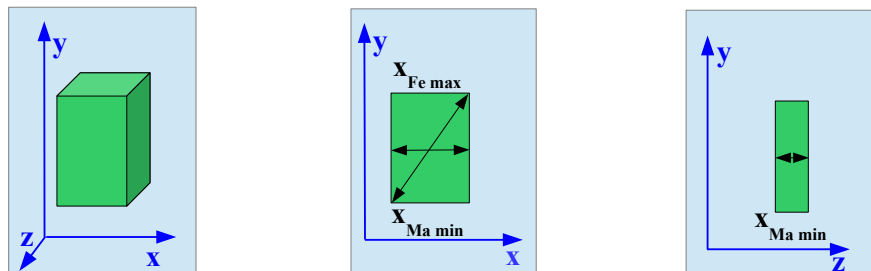
$$q_3(x_{M a m i n}) = \frac{dQ_3(x_{M a m i n})}{dx_{M a m i n}}. \quad (6)$$

140 The characteristic diameters, obtained from sieving and 2D dynamic imag-
141 ing, were defined based on three sizes within the entire population: d10,
142 d50, d90. The d50 value is the median particle size within the population,
143 with 50 % of the population greater than this size, and 50 % smaller than this
144 size. Similarly, 10 % of the population is smaller than the d10 size; while 90 %
145 of the population is smaller than the d90 size [22]. All measurements were
146 conducted in triplicate to establish repeatability which exceeded 95 % confi-
147 dence intervals, as shown in the Supplemental material. The measurement
148 inaccuracy from sieving analysis was mainly caused by weighing errors.

149 *Light microscopy.* Light microscopy of sawdust and disintegrated pellets was
150 conducted using a 1750 microscope heating stage (Leica Microsystems, Ger-
151 many) in order to characterize the particle shape. Digital images were cap-
152 tured using a camera attached to the microscope and then analyzed using the
153 software that incorporates a simple ruler. The particle geometric parameters
154 were measured manually using appropriate diameter definitions. At least 440
155 particles are required to obtain 10 particles in each fraction for statistically
156 reliable results. In the microscopy analysis, about 500 biomass particles were

1
2
3
4
5
6
7
8
9
10
11
12
13
14
15
16
17
18
19
20
21
22
23
24
25
26
27
28
29
30
31
32
33
34
35
36
37
38
39
40
41
42
43
44
45
46
47
48
49
50
51
52
53
54
55
56
57
58
59
60
61
62
63
64
65

157 characterized. The width and length of a biomass particle were analyzed using
158 a ruler in the microscope's software. Smaller particles were analyzed on
159 a piece of adhesive tape. A single biomass particle was manually rotated by
160 90° in the sample plane to determine all three dimensions.



3(a): Biomass particle

3(b): Width and length

3(c): Thickness

Figure 3: Measurement of particle three dimensions (width, length, thickness) by the light microscopy.

161 *Laser diffraction.* The particle size distribution of biomass samples was de-
162 termined by a 2000 particle size analyzer (Malvern Instruments Ltd, UK)
163 using a wet method. The biomass samples were dispersed in ethanol. All
164 measurements were made at room temperature and at 3200 rpm on at least
165 two samples. The refractive indices of biomass and ethanol were taken as
166 1.53 and 1.33, respectively [23]. The Sauter mean diameter was calculated as
167 the surface area moment mean, and defined as

$$D_{32} = \frac{\sum n_i d_i^3}{\sum n_i d_i^2}. \quad (7)$$

168 The volume mean diameter (D_{43}) was calculated as follows

$$D_{43} = \frac{\sum n_i d_i^4}{\sum n_i d_i^3}, \quad (8)$$

1
2
3
4
5
6
7
8
9 where n_i is the number of particles with measured diameter d_i .

10
11
12 *Focused beam reflectance measurement.* The particle size distribution was
13
14 determined using a G400 focused beam reflectance analyzer (Mettler Toledo,
15
16 UK). The focused beam of laser light scans across individual particles at a
17
18 fixed scan speed [24]. The backscattered light is detected as a signal issued
19
20 from one particle edge to an opposing edge. The pulse signal duration is
21
22 multiplied by the scan speed to calculate the chord length.

23
24 A 1 g of biomass was added to a 200 ml glass beaker filled with methanol.
25
26 The biomass particles were stirred using an anchor type stirrer at 200 rpm at
27
28 room temperature. Five measurements, each of 15 min duration, were made
29
30 on each sample, and the data was recorded using the FBRM acquisition soft-
31
32 ware. The chord lengths, in the range of 1 to 1000 μm , were split into ninety
33
34 classes ($N = 90$). The total number of counts per class (n_i) is determined as

35
36
37
38
39
40
41
42
43
44
45
46
47
48
49
50
51
52
53
54
55
56
57
58
59
60
61
62
63
64
65

$$n_{total} = \sum_1^N n_i. \quad (9)$$

182 The results of a particle size analysis by FBRM are always presented as an
183 unweighted chord length distribution. For any particle shape, the number
184 of small chord length counts statistically outweighs the large particle chord
185 length counts [25]. The class weighting was used in order to emphasize the
186 longer chords, which represent the most likely lengths of wood fibers. A class-
187 specific weight (w_i) to the number of counts (n_i) is then used to calculate
188 weighted chord length so that

$$L_i = w_i \cdot n_i. \quad (10)$$

1
2
3
4
5
6
7
8
9
10
11
12
13
14
15
16
17
18
19
20
21
22
23
24
25
26
27
28
29
30
31
32
33
34
35
36
37
38
39
40
41
42
43
44
45
46
47
48
49
50
51
52
53
54
55
56
57
58
59
60
61
62
63
64
65

189 The weights (w_i) are obtained from the class midpoint (M_i)

$$w_i = \frac{M_i^j}{\sum_{i=1}^N M_i^j} \cdot N. \quad (11)$$

190 In equation 11, $j=0$ and $j=2$ are unweighted and square-weighted particle size
191 distributions, respectively. The raw chord length data ($j=0$) is first collected
192 by the FBRM probe, and then weighted using the square-weighting function.
193 The mean chord length on a square-weighted basis is calculated as

$$\bar{L} = \frac{\sum_{i=1}^N n_i M_i^3}{\sum_{i=1}^N n_i M_i^2}. \quad (12)$$

194 Similar to volume-weighted distributions, the square-weighted distributions
195 are sensitive to the amount of large particles. The square-weighted mean
196 chord length is equivalent to the Sauter mean diameter [26–28]. The results
197 of a particle size analysis are presented as a square-weighted frequency dis-
198 tribution and calculated as

$$q_3(L) = \frac{n_i L_i^2}{\sum_{i=1}^N (n_i L_i^2)}. \quad (13)$$

199 The FBRM results of Heath et al. [27] showed that the square-weighting is
200 effectively a cube (volume) weighting and is comparable to the volume-based
201 distribution used in laser diffraction.

202 **3. Results**

203 *3.1. Particle size analysis*

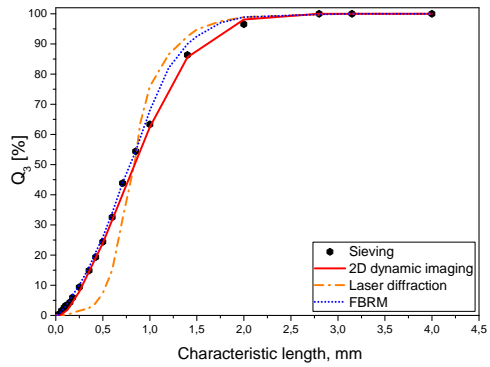
204 Because of the coupling between chemistry and heat and mass transfer
205 during particle conversion, fuel particle size has a noticeable effect on com-

1
2
3
4
5
6
7
8
9
10
11
12
13
14
15
16
17
18
19
20
21
22
23
24
25
26
27
28
29
30
31
32
33
34
35
36
37
38
39
40
41
42
43
44
45
46
47
48
49
50
51
52
53
54
55
56
57
58
59
60
61
62
63
64
65

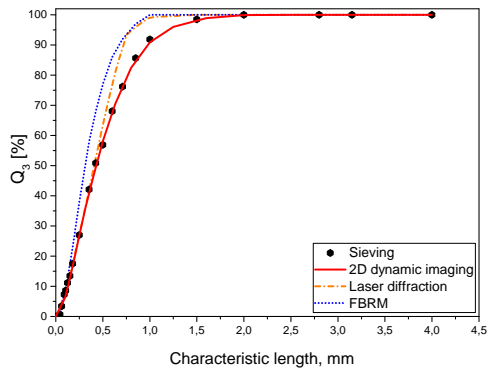
206 bustion process characteristics. Thus, the choice of the suitable particle size
207 descriptors is relevant. In 2D dynamic imaging, the minimal Martin diameter
208 ($x_{M a m i n}$) represents a particle width, which is larger than its thickness. The
209 Feret maximal diameter, representing the length, is greater than the width.
210 Therefore, the Martin minimal ($x_{M a m i n}$) and Feret maximal ($x_{F e m a x}$) diam-
211 eters are suitable parameters to represent the width and length of biomass
212 particles, confirming previous results of Trubetskaya et al. [29].

213 The most suitable descriptor of particle size, when characterized using
214 sieving and 2D dynamic imaging, is the smallest maximal chord ($x_{c m i n}$) [19].
215 The difference between particle size distributions over $x_{M a m i n}$ and $x_{c m i n}$ di-
216 ameters is small as shown in Supplementary Figure S-5. Thus, the particle
217 width can be represented by $x_{c m i n}$ diameter when the 2D dynamic imaging
218 device is not available. Figure 4 shows particle size distributions for poplar,
219 pulverized wood sample and wheat straw, characterized using the sieving, 2D
220 dynamic imaging, laser diffraction and focused beam reflectance technique.

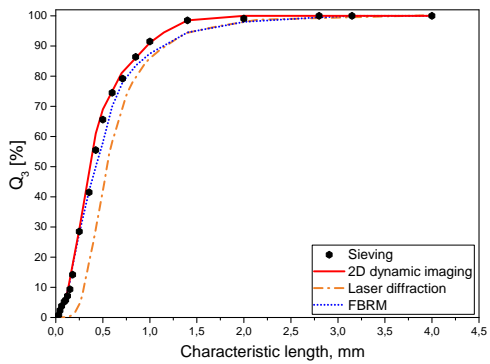
1
2
3
4
5
6
7
8
9
10
11
12
13
14
15
16
17
18
19
20
21
22
23
24
25
26
27
28
29
30
31
32
33
34
35
36
37
38
39
40
41
42
43
44
45
46
47
48
49
50
51
52
53
54
55
56
57
58
59
60
61
62
63
64
65



4(a): Poplar



4(b): Pulverized wood



4(c): Wheat straw

Figure 4: Cumulative particle size distribution Q_3 , based on volume, for poplar, pulverized wood and wheat straw samples characterized by the sieving, 2D dynamic imaging ($x_{Ma,min}$), laser diffraction and focused beam reflectance technique.

1
2
3
4
5
6
7
8
9
221 The data obtained by different particle size characterization techniques is
10
222 repeatable, as shown in the Supplemental material. The particle size analysis
11
12
13 223 indicated that pulverized wood contained a larger fraction of small particles
14
15 224 compared to poplar and wheat straw. The poplar particle size distribution
16
17 225 was more heterogeneous than those of other fuels. Figure 4 shows that siev-
18
19 226 ing and 2D dynamic imaging produced very similar size distributions for all
20
21 227 biomass samples, while a significant deviation was observed when compared
22
23 228 with the results from the laser diffraction and the FBRM.

24
25 229 The 2D dynamic imaging captures the shadows of randomly orientated
26
27 230 3D particles. 2D projections of a 3D particle and their dependency on the
28
29 231 orientation and shape can be recorded by CAMSIZER cameras in various
30
31 232 ways. Gil et al. [30] reported that sieve size corresponds to biomass particle
32
33 233 width (shorter dimension) with sieving efficiency around 70 % depending on
34
35 234 the feedstock and considered size fraction. The square-shaped sieve aper-
36
37 235 tures allow the passage of about 0.8 times the width of the particle [31].
38
39 236 During sieving, particles always fall through the sieves with their smallest
40
41 237 two-dimensional projection, which does not appear the case for biomass par-
42
43 238 ticles. In 2D dynamic imaging of elongated biomass particles, the width
44
45 239 of a particle projection does not change significantly, while the length of a
46
47 240 particle is strongly influenced by the particle rotation / orientation in the
48
49 241 measurement shaft. The x_{Mamin} diameter does not change as extensively as
50
51 242 the x_{cmin} . The sieving curve was close to the 2D dynamic imaging curve
52
53 243 representing x_{Mamin} particle model for all samples. Overall, sieving is more
54
55 244 convenient when a large biomass sample quantity has to be analyzed and
56
57 245 when the particle size exceeds the measurement limitations of other sizing

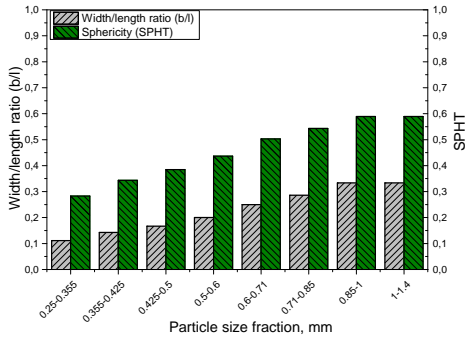
1
2
3
4
5
6
7
8
9 246 techniques, while 2D dynamic imaging is recommended when information
10
11 247 about particle shape is required.

12
13 248 Particle size distributions measured by 2D dynamic imaging deviate sig-
14
15 249 nificantly from those obtained using the FBRM device. 2D dynamic imaging
16
17 250 evaluates the particle size based on attributes of non-spherical shapes. The
18
19 251 FBRM device measures chord lengths, where a chord length is defined as a
20
21 252 straight line between any two points on the edge of a particle. The accuracy
22
23 253 of particle size characterization using the FBRM device might be influenced
24
25 254 by the various shapes of a biomass particle with broken edges. The results of
26
27 255 the laser diffraction analysis showed that both poplar and wheat straw sam-
28
29 256 ples contained a larger fraction of coarse particles - a result which was not
30
31 257 in agreement with other size characterization techniques. The difference be-
32
33 258 tween the particle size distributions measured by the laser diffraction and the
34
35 259 other techniques is large. Since biomass particle shapes deviate significantly
36
37 260 from a sphere, the spherical assumptions in the optical models are not valid.
38
39 261 Thus, the results of the laser diffraction analysis do not characterize the real
40
41 262 size of biomass particles. The discrepancy was partly due to the fact that the
42
43 263 laser diffraction measures the diameters of equivalent volume particles from
44
45 264 the diffraction signals [32–35]. The wrong assumption of random orientation
46
47 265 of fibers in the laser diffraction affects measurement accuracy [32, 36].

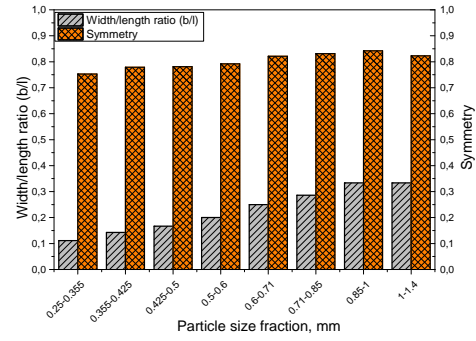
48 266 *3.2. Particle shape analysis*

49

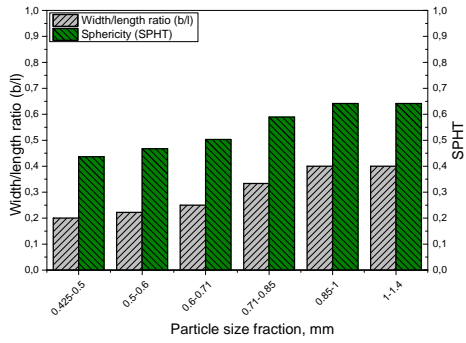
50
51 267 The particle shape was characterized using both the 2D dynamic imag-
52
53 268 ing instrument and light microscopy. The small biomass particles of size $<$
54
55 269 0.5 mm were more elongated (SPHT = 0.31 and aspect ratio AR = 0.11), as
56
57 270 shown in Figure 5.



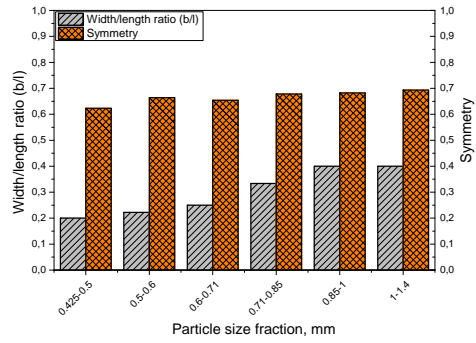
5(a): Poplar sphericity



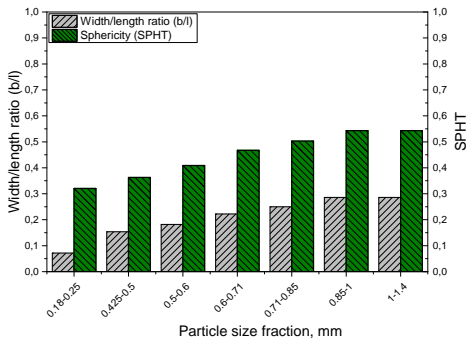
5(b): Poplar symmetry



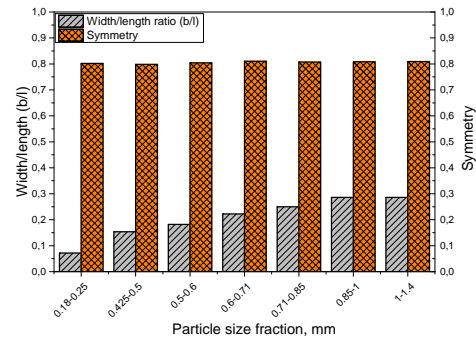
5(c): Pulverized wood sphericity



5(d): Pulverized wood symmetry



5(e): Wheat straw sphericity



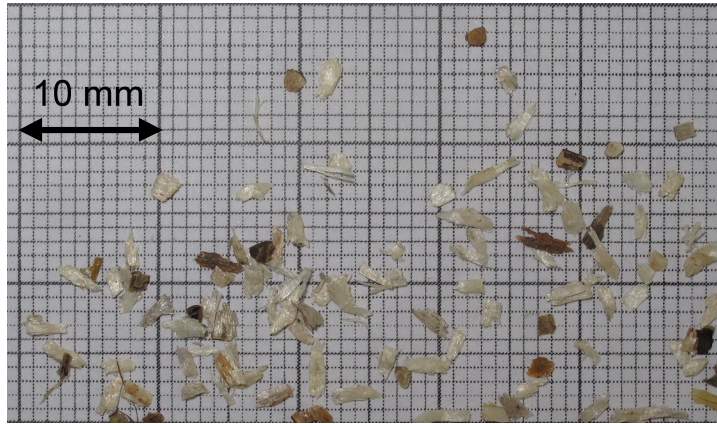
5(f): Wheat straw symmetry

Figure 5: Shape factors (sphericity/circularity and symmetry) in comparison to the aspect ratio (b/l) of poplar, pulverized wood and wheat straw samples which were sieved to the 0.71-1 mm fraction, and characterized by 2D dynamic imaging.

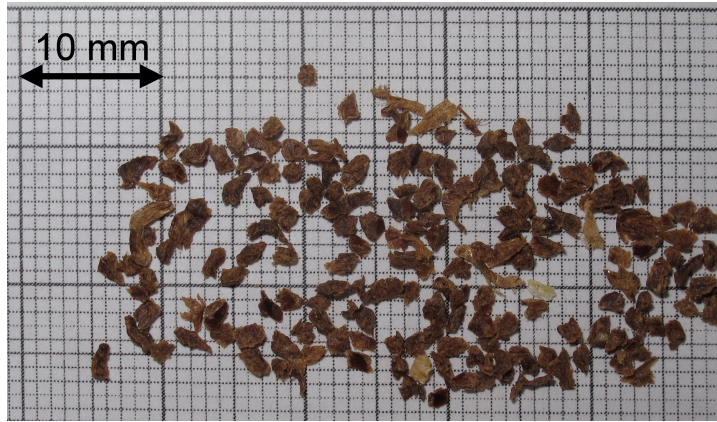
1
2
3
4
5
6
7
8
9
10 271 The aspect ratio of biomass particles measured by 2D dynamic imaging
11 272 over $x_{M_{amin}}$ decreased from 0.25 to 0.11 with decreasing particle size, indi-
12
13 273 cating that larger particles exhibited a more elongated shape. The sphericity
14
15 274 (mean SPHT of all samples = 0.51) and the aspect ratio (mean AR of all
16
17 275 samples = 0.32) for particle fractions > 0.5 mm indicate that they were more
18
19 276 square-shaped. Symmetries of poplar and wheat straw particles were similar;
20
21 277 particles were polygonal and symmetrical with holes (Symm = 0.8). Com-
22
23 278 pared to the poplar and wheat straw samples, the pulverized wood showed
24
25 279 a stronger anisotropy in shape (Symm = 0.68), which might be caused by
26
27 280 the particle edge deformation during secondary comminution. Overall, 2D
28
29 281 dynamic imaging analysis showed that the particles of a different size had
30
31 282 similar rectangular shapes and that the ratio between particle dimensions did
32
33 283 not change significantly with decreasing particle size, which is in line with
34
35 284 the results of Cardoso et al. [37].

36 285 In Figure 6, the light microscopy results show elongated wheat straw
37
38 286 particles. The main difference among the fuels was that the pulverized wood
39
40 287 formed more square-shaped particles while the particles of poplar and wheat
41
42 288 straw were elongated, confirming the results of 2D dynamic imaging in Fig-
43
44 289 ure 5. There was little change in the average particle shape among the size
45
46 290 classes.

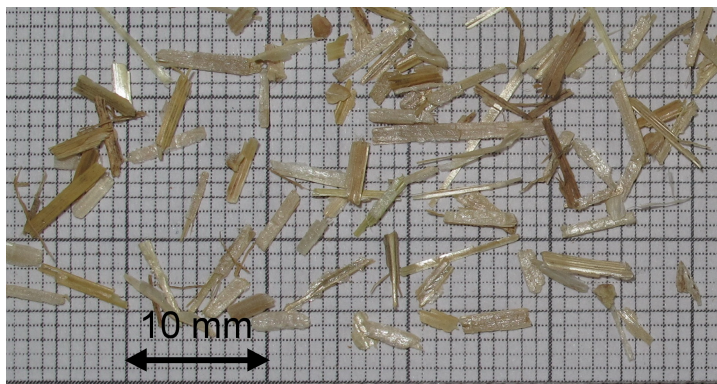
1
2
3
4
5
6
7
8
9
10
11
12
13
14
15
16
17
18
19
20
21
22
23
24
25
26
27
28
29
30
31
32
33
34
35
36
37
38
39
40
41
42
43
44
45
46
47
48
49
50
51
52
53
54
55
56
57
58
59
60
61
62
63
64
65



6(a): Poplar



6(b): Pulverized wood



6(c): Wheat straw

Figure 6: Light microscopy images of (a) poplar, (b) pulverized wood and (c) wheat straw particles.

1
2
3
4
5
6
7
8
9
291 The major drawback of the 2D dynamic imaging is that two-dimensional
10
11 292 projections can be generated only. Consequently, the third dimension cannot
12
13 293 be obtained, and for the particle volume calculation, the thickness is often
14
15 294 assumed to be equal to the width. In order to examine the accuracy of this
16
17 295 simplification, the biomass particles were analyzed using 2D dynamic imaging
18
19 296 and light microscopy. In terms of absolute accuracy, the microscopy provides
20
21 297 a high resolution and high magnification images, but they only represent a
22
23 298 small sample amount.

24
25 299 The 2D dynamic imaging results, together with the light microscopy
26
27 300 data, are shown in Supplementary Figure S-6. In the light microscopy anal-
28
29 301 ysis, $x_{M a m i n}$ and $x_{F e m a x}$ were determined manually to make the data from
30
31 302 both techniques comparable. A significant difference was observed in particle
32
33 303 length, represented by $x_{F e m a x}$, while the deviations in the width, represented
34
35 304 by $x_{M a m i n}$, were almost negligible. The particle alignment has more influence
36
37 305 on the measurement in 2D dynamic imaging. During the microscopy analy-
38
39 306 sis, particles were aligned perpendicular to the measurement direction, and
40
41 307 thus, the particle alignment only slightly influenced the particle size. The ob-
42
43 308 servation made by Igathinathane et al. [38] that the measured length depends
44
45 309 on orientation angle in imaging analysis was confirmed in the present study.
46
47 310 It was shown [38], that correction factors can rectify the overestimation. The
48
49 311 microscopy and 2D dynamic imaging results with respect to $x_{F e m a x}$ can be
50
51 312 made comparable if the results from the imaging analysis are multiplied by
52
53 313 $\cos(45^\circ)$ [39], as shown in Supplementary Figure S-6.

54
55 314 Igathinathane et al. [38] used the $\sqrt{\pi}/2$ (≈ 0.886) correction factor to
56
57 315 reduce the width and length of rectangular and cubic particles in imaging

1
2
3
4
5
6
7
8
9
316 analysis; the factor is close to the correction factor of $\cos(45^\circ) \approx 0.707$.
10
11 In 2D dynamic imaging software, the particle thickness is assumed to be
12
13 318 equal to the width. The present microscopy results show that the particle
14
15 319 thickness of woody and herbaceous feedstocks can be estimated to be 2/3
16
17 320 of the particle width ($x_{Ma\ min}$), as shown in Supplementary Figure S-7. The
18
19 321 thickness of larger (> 0.6 mm) wheat straw and pulverized wood particles
20
21 322 can be estimated as 1/2 of the particle's width, confirming the results of
22
23 323 Momeni [40].
24

25 324 *3.3. Representation of biomass particle shape in modeling*

26
27
28 325 In suspension firing, biomass particles undergo rapid heating, drying
29
30 326 and devolatilization with the formation of char and volatiles. Devolatilization
31
32 327 models often assume non-isothermal biomass particles, and include external
33
34 328 and internal heat transfer [17]. A non-isothermal model has been developed
35
36 329 to estimate the yields of volatiles and char at different heating rates, high
37
38 330 temperatures (up to 1500°C) and is valid for different biomass particle sizes.
39
40 331 The particle model was validated against data from separate pyrolysis exper-
41
42 332 iments performed at an intermediate heating rate ($10\text{-}10^3$ K s $^{-1}$) in the wire
43
44 333 mesh reactor (WMR) and at a high heating rate of (10^4 K s $^{-1}$) in the drop
45
46 334 tube reactor (DTF) [41]. A particle enters a hot gas stream and is heated
47
48 335 up by convection and radiation. The unsteady heat conduction equation
49
50 336 (Fourier's Law) in cylindrical coordinates (f=1) is used:

$$51 \quad c_{p,s} \cdot \frac{dT_p}{dt} = \frac{1}{\rho_s} \cdot \frac{1}{r^f} \cdot \frac{\partial}{\partial r} \left(r^f \lambda_{eff} \frac{\partial T_p}{\partial r} \right) \quad (14)$$

52
53
54 337 The parameters in equation 14 are defined in nomenclature. The effective
55
56 338 thermal conductivity (λ_{eff}) inside the particle is approximated by Bellais
57
58

1
2
3
4
5
6
7
8
9 and Grønli [42, 43]. A biomass particle can be represented as a plate, a
10 cylinder and a sphere in planar (f=0), cylindrical (f=1), and spherical (f=2)
11 coordinates under the assumption of similar volume to surface ratios using a
12 different characteristic length:
13
14
15
16

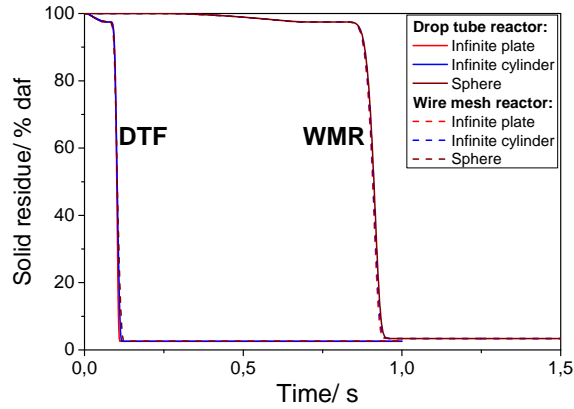
$$17 \quad d_p = x_{M_{a \min}} \quad (\text{cylinder}) \quad (15)$$

$$18 \quad d_p = \frac{1}{2} \cdot x_{M_{a \min}} \quad (\text{plate}) \quad (16)$$

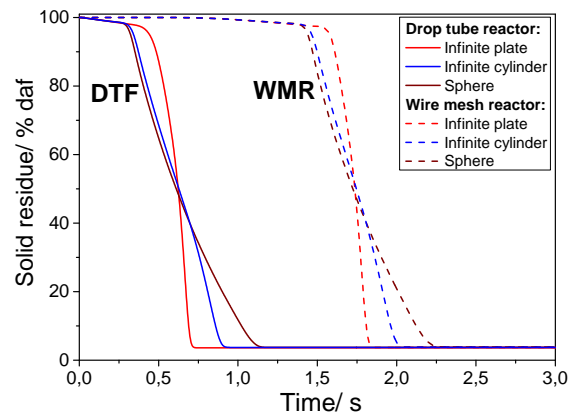
$$19 \quad d_p = \frac{3}{2} \cdot x_{M_{a \min}} \quad (\text{sphere}) \quad (17)$$

20
21
22
23
24
25 As it has been shown in this work, biomass particles possess large aspect ra-
26 tios so that a spherical representation should be avoided. A cylindrical shape
27 allows treatment of biomass particles as one-dimensional [9]. Thus, it is rec-
28 ommended to represent biomass particles as infinite cylinders, corresponding
29 to f=1 with a particle size equal to $x_{M_{a \min}}$, as shown in equation 15.
30
31
32
33
34

35 Figure 7 illustrates the mass loss of 0.2 and 1 mm pulverized wood parti-
36 cles. The previous results from the 1D model emphasized a key role of intra-
37 particle heat conduction in biomass particle > 0.25 mm [41]. Devolatilization
38 time decreased with the higher heating rate in the drop tube reactor com-
39 pared to the wire mesh reactor. The representation of the 0.2 mm particles
40 using different characteristics lengths does not give large deviations with
41 respect to char yield and devolatilization time among the three particle ge-
42 ometries as shown in Figure 7(a).
43
44
45
46
47
48
49
50
51
52
53
54
55
56
57
58
59
60
61
62
63
64
65



7(a): Pulverized wood 0.2 mm



7(b): Pulverized wood 1 mm

Figure 7: Mass loss histories of pulverized wood particles (0.2 and 1 mm) with the similar volume to surface ratio and different characteristic lengths which were calculated in plate-like ($n=0$), cylindrical ($n=1$) and spherical ($n=2$) geometries at the final temperature of 1400°C during pyrolysis in the wire mesh and drop tube reactors.

356

The influence of particle shape becomes more important with the in-

1
2
3
4
5
6
7
8
9
10 357 creasing particle size due to the larger internal temperature gradients as
11 358 shown in Figure 7(b). The relative influence of heating rate on devolatiliza-
12
13 359 tion time of 1 mm pulverized wood was less as compared to that for smaller
14
15 360 particles. This is because of the predominance of internal heat transfer con-
16
17 361 trol within the large particles.

18 19 20 362 *3.4. Discussion*

21
22 363 Prior to combustion modeling, biomass samples are usually analyzed to
23
24 364 obtain the shape parameters (i.e. the sphericity, symmetry and aspect ra-
25
26 365 tio) by using one of the discussed techniques. Various biomass shapes result
27
28 366 in different volume-to-surface area ratios which determine heat and mass
29
30 367 transfer [9, 44]. A spherical particle, as commonly used in literature [45],
31
32 368 has a higher volume to surface area ratio than a cylindrical particle of the
33
34 369 same volume. Therefore, particles with a smaller aspect ratio heat up faster,
35
36 370 which results in a faster conversion rate. The experimental investigations
37
38 371 showed significantly smaller aspect ratios of biomass particles compared to
39
40 372 coal, indicating that the spherical representation of a biomass particle (larger
41
42 373 volume-to-surface area ratios) overestimates devolatilization time, for exam-
43
44 374 ple.

45
46 375 Lu et al. [9, 46] measured and calculated particle surface area and vol-
47
48 376 ume using a three-dimensional particle shape reconstruction algorithm based
49
50 377 on three images taken from orthogonal directions. The particle surface and
51
52 378 volume calculation involved image acquisition and processing, image contour
53
54 379 alignment and surface generation. In the present study, particle size distri-
55
56 380 butions obtained by 2D dynamic imaging were used to calculate the volume
57
58 381 to surface ratio, where x_{Mamin} diameter was used as the particle width. The

1
2
3
4
5
6
7
8
9
382 x_{Mamin} diameter can be replaced by x_{cmin} when a 2D dynamic imaging de-
10
11 vice is not available, since only small differences occur while representing
12
13 384 particle size distributions, based on volume, over x_{Mamin} and x_{cmin} diame-
14
15 385 ters. Alternatively, the average specific surface area can be measured by 2D
16
17 386 dynamic imaging, and multiplied by the $\cos(45^\circ)$ factor.

18
19 387 In particle technology, a particle is often represented as an ellipsoid,
20
21 388 based on favorable properties such as geometric interlocking and an accurate
22
23 389 description of convex particle shapes [47]. In addition, an ellipsoid resem-
24
25 390 bles a large array of shapes, including that of a flake like particle (oblate
26
27 391 ellipsoid) and a rod-like particle (prolate ellipsoid) [11]. In the mathematical
28
29 392 combustion model, a complete char burnout is a common assumption, so
30
31 393 that a rectangular shape can be chosen as the best particle shape descrip-
32
33 394 tor since the rectangular-shaped particles demonstrate the longest burnout
34
35 395 times. However, the ellipsoidal and rectangular representations are very diffi-
36
37 396 cult to model. The cylindrical representation may give a precise description of
38
39 397 char burnout, although the particle volume, compared to the ellipsoidal vol-
40
41 398 ume, with equal dimensions tends to be overestimated by the minimal time
42
43 399 required for the mass and heat transfer calculations. Moreover, the cylin-
44
45 400 drical representation does not consider the biomass particles' edges, which
46
47 401 influence the heat and mass transfer calculation in combustion modeling.

402 **4. Conclusion**

403 An experimental study was carried out to investigate the particle size
404 and shape characteristics of woody and herbaceous biomass. The particle
405 size results obtained by 2D dynamic imaging were in agreement with the

1
2
3
4
5
6
7
8
9
10 406 sieving data. A significant disparity was observed in the laser diffraction and
11 407 the focused beam reflectance measurements. 2D dynamic imaging was found
12
13 408 to be the most convenient characterization method, providing additional in-
14
15 409 formation on particle shape and external surface area. Light microscopy and
16
17 410 2D dynamic imaging showed that pulverized wood formed square-shaped
18
19 411 particles, while the poplar and wheat straw particles were elongated and of
20
21 412 rectangular-shape. It is recommended to represent biomass particles in com-
22
23 413 bustion models as infinite cylinders, where the particle width is represented
24
25 414 either by $x_{Ma\ min}$ or $x_{c\ min}$ diameters. The relative influence of heating rate
26
27 415 on devolatilization time of larger wood particles was less as compared to that
28
29 416 for smaller particles, whereas the influence of particle shape became more im-
30
31 417 portant with the increasing particle size due to the predominance of internal
32
33 418 heat transfer control within the large particles.

35 419 **Acknowledgements**

36
37
38 420 The authors would like to acknowledge the financial support received
39
40 421 from the Danish Strategic Research Council (Grant Nr. DSF-10-093956),
41
42 422 Kempestiftelse, DONG Energy, Vattenfall and HOFOR. We would like also
43
44 423 to thank Ian Haley and Brian O'Sullivan from Mettler Toledo for assist-
45
46 424 ing with FBRM measurements. The authors thank DTU Combustion and
47
48 425 Harmful Emission Control group for the fruitful discussions. Erika Christ
49
50 426 are acknowledged for the article proof reading.

1
2
3
4
5
6
7
8
9 **References**

- 10
11
12 428 [1] Saleh SB, Hansen BB, Jensen PA, Dam-Johansen K, Influence of
13 429 Biomass Chemical Properties on Torrefication Characteristics, *Energy*
14 430 *Fuels* 27 (2013) 7541–8.
- 15
16
17
18 431 [2] Spinelli R, Cavallo E, Facello A, Magagnotti N, Nati C, Paletto G,
19 432 Performance and energy efficiency of alternative comminution principles:
20 433 Chipping versus grinding, *Scan J Forest Research* 27 (2012) 393–400.
- 21
22
23
24 434 [3] Mandø M, Rosendahl L, Yin C, Sørensen H, Pulverized straw combus-
25 435 tion in a low NO_x multifuel burner: Modeling the transition from coal
26 436 to straw, *Fuel* 89 (2010) 3051–62.
- 27
28
29
30 437 [4] Abbas T, Costen PG, Lockwood FC, Solid fuel utilization: from coal to
31 438 biomass, *Proc 26th Int Symp Comb* (1996) 3041–58.
- 32
33
34
35 439 [5] Tamura M, Watanabe S, Kotake N, Hasegawa M, Grinding and combus-
36 440 tion characteristics of woody biomass for co-firing with coal in pulverised
37 441 coal boilers, *Fuel* 134 (2014) 544–53.
- 38
39
40
41 442 [6] Rosendahl L, Using a multi-parameter particle shape description to pre-
42 443 dict the motion of non-spherical particle shape in swirling flow, *Appl*
43 444 *Math Model* 24 (2000) 11–25.
- 44
45
46
47 445 [7] Thunman H, Leckner B, Niklasson F, Johnsson F, Combustion of wood
48 446 particles - a particle model for eulerian calculations, *Combust Flame*
49 447 129 (2002) 30–46.
- 50
51
52
53
54
55
56
57
58
59
60
61
62
63
64
65

1
2
3
4
5
6
7
8
9
10
11
12
13
14
15
16
17
18
19
20
21
22
23
24
25
26
27
28
29
30
31
32
33
34
35
36
37
38
39
40
41
42
43
44
45
46
47
48
49
50
51
52
53
54
55
56
57
58
59
60
61
62
63
64
65

448 [8] Saastamoinen J, Aho M, Moilanen A, Sørensen LH, Clausen S, Berg
449 M, Burnout of pulverized biomass particles in large scale boiler - Single
450 particle model approach, *Biomass Bioenergy* 34 (2010) 728–36.

451 [9] Lu H, Ip E, Scott J, Foster P, Vickers M, Baxter LL, Effect of particle
452 shape and size on devolatilization of biomass particles, *Fuel* 89 (2010)
453 1156–68.

454 [10] Ma L, Jones JM, Pourkashanian M, Williams A, Modelling the combus-
455 tion of pulverized biomass in an industrial combustion test furnace, *Fuel*
456 86 (2007) 1959–65.

457 [11] Mandø M, Turbulence Modulation by Non-Spherical Particles. PhD the-
458 sis, Aalborg University (2009).

459 [12] German RM, Powder Metal Science, Metal Powder Industries Federa-
460 tion, 1984.

461 [13] Yin C, Rosendahl L, Condra TJ, Use of numerical modeling in design for
462 co-firing biomass in wall-fired burners, *Chem Eng Sci* 59 (2004) 3281–92.

463 [14] Yang YB, Sharifi VN, Swithenbank J, Williams A, Combustion of a
464 Single Particle of Biomass, *Chemosphere* 42 (2001) 481–90.

465 [15] Sannigrahi P, Ragauskas AJ, Tuskan GA, Poplar as a feedstock for bio-
466 fuels: A review of compositional characteristics, *Biofuels Bioprod Bioref*
467 4 (2010) 209–26.

468 [16] Trubetskaya A, Jensen PA, Jensen AD, Steibel M, Spliethoff H, Glar-
469 borg P, Influence of fast pyrolysis conditions on yield and structural

1
2
3
4
5
6
7
8
9
10
11
12
13
14
15
16
17
18
19
20
21
22
23
24
25
26
27
28
29
30
31
32
33
34
35
36
37
38
39
40
41
42
43
44
45
46
47
48
49
50
51
52
53
54
55
56
57
58
59
60
61
62
63
64
65

470 transformation of biomass char, *Fuel Process Technol* 140 (2015) 205–
471 14.

472 [17] Trubetskaya A, Fast pyrolysis of biomass at high temperatures. PhD
473 thesis, Technical University of Denmark (2016).

474 [18] Stuess M, *Mechanische Verfahrenstechnik 1* (in German), Springer, 1992.

475 [19] Merkus HG, *Particle Size Measurements*, Springer, 2009.

476 [20] Saad ES, Mostafa ME, Analysis of Grain Size Statistic and Particle Size
477 Distribution, *Waste Biomass Valor* 5 (2014) 1005–18.

478 [21] Williams O, Newbolt G, Eastwick C, Kingman S, Giddings D, Lester E
479 et al., Influence of mill type on densified biomass comminution, *Applied*
480 *Energy* 182 (2016) 219–31.

481 [22] Tannous K, Lam PS, Sokhansanj S, Grace JR, Physical properties for
482 flow characterization of ground biomass from Douglas Fir Wood, *Part*
483 *Sci Technol* 31 (2012) 291–300.

484 [23] Gavlighi HA, Meyer AS, Zaidel DNA, Mohammadifar MA, Mikkelsen
485 JD, Stabilization of emulsions by gum tragacanth (*Astragalus* spp.) core-
486 lates to the galacturonic acid content and methoxylation degree of the
487 gum, *Food Hydro* 31 (2013) 5–14.

488 [24] Maass S, Wollny S, Voigt A, Kraume M, Experimental comparison of
489 measurement techniques for drop size distribution in liquid/liquid dis-
490 persions, *Experiments Fluids* 50 (2) (2011) 259–69.

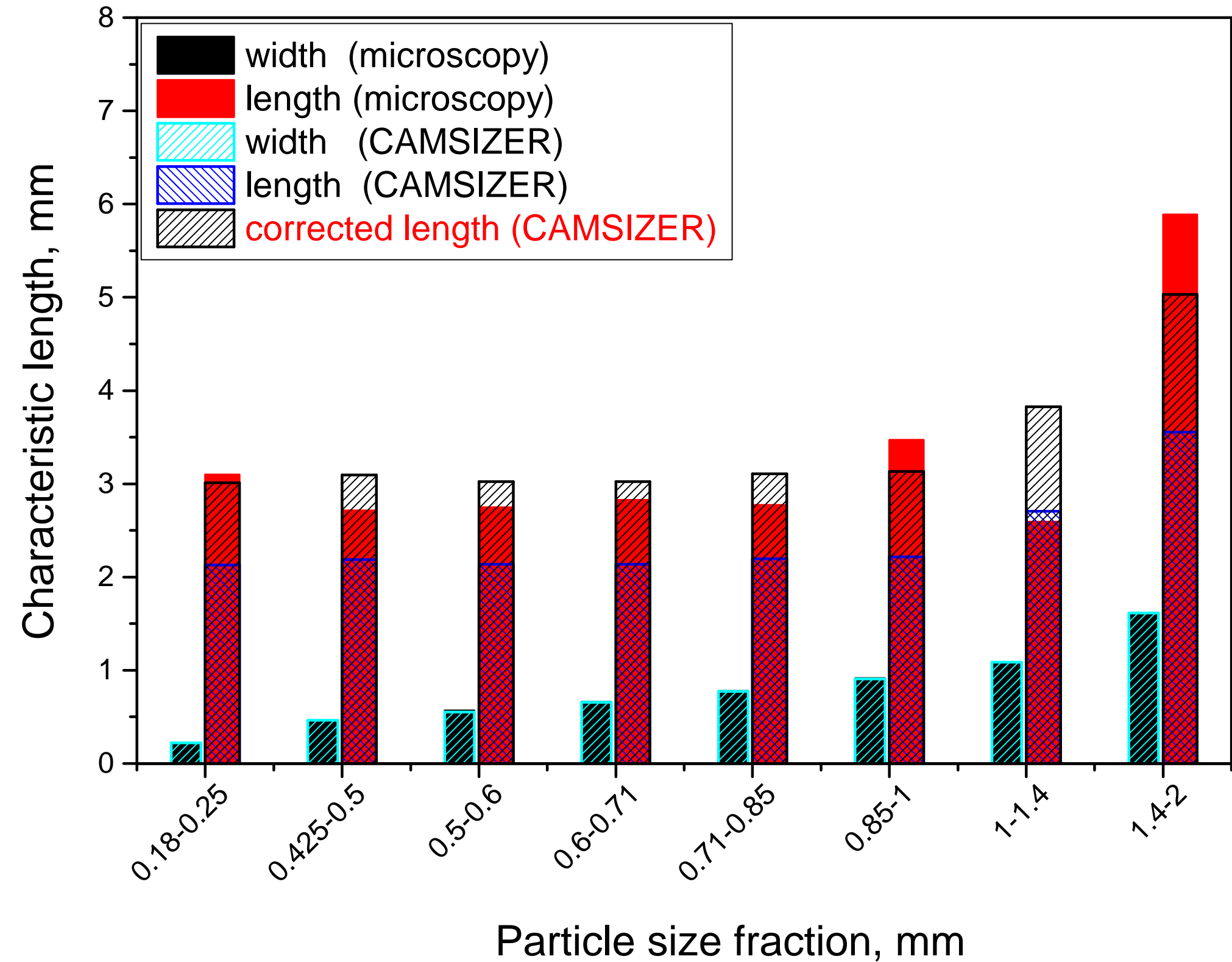
- 1
2
3
4
5
6
7
8
9
10 491 [25] Leyssens T, Baudry C, Escudero Hernandez ML, Optimization of Crystallization by Online FBRM Analysis of Needle-Shaped Crystals, *Org*
11 492 *Process Res* 15 (2) (2011) 413–26.
12
13 493
14
15 494 [26] Clain P, Ndoye FT, Delahaye A, Fournaison L, Lin W, Dalmazzone D,
16
17 495 Particle size distribution of TBPB hydrates by focused beam reflectance
18
19 496 measurement (FBRM) for secondary refrigeration application, *Int J Re-*
20
21 497 *frige* 50 (2015) 19–31.
22
23
24 498 [27] Heath AR, Fawell PD, Bahri PA, Swift JD, Estimating Average Particle
25
26 499 Size by Focused Beam Reflectance Measurement (FBRM), *Part Part*
27
28 500 *Syst Charact* 19 (2002) 84–95.
29
30
31 501 [28] Schümann H, Tutkun M, Nydal OJ, Experimental study of dispersed
32
33 502 oil-water flow in a horizontal pipe with enhanced inlet mixing, Part 2:
34
35 503 In-situ droplet measurements, *J Petrol Sci Eng* 145 (2016) 753–62.
36
37 504 [29] Trubetskaya A, Poyraz Y, Weber R, Wadenbäck J, Secondary comminution
38
39 505 of wood pellets in power plant and laboratory-scale mills, *Fuel Process*
40
41 506 *Tech* 160 (2017) 216–27.
42
43
44 507 [30] Gil M, Teruel E, Arauzo I, Analysis of standard sieving method for
45
46 508 milled biomass through image processing. Effects of particle shape and
47
48 509 size for poplar and corn stover, *Fuel* 116 (2014) 328–40.
49
50 510 [31] Dhir RK, McCarthy MJ, *Concrete durability and repair technology*,
51
52 511 Thomas Telford, 1999.
53
54 512 [32] Kelly RN, Di Sante KJ, Stranzl E, Kazanjian JA, Bowen P, Matsuyama
55
56 513 T et al., Graphical comparison of image analysis and laser diffraction

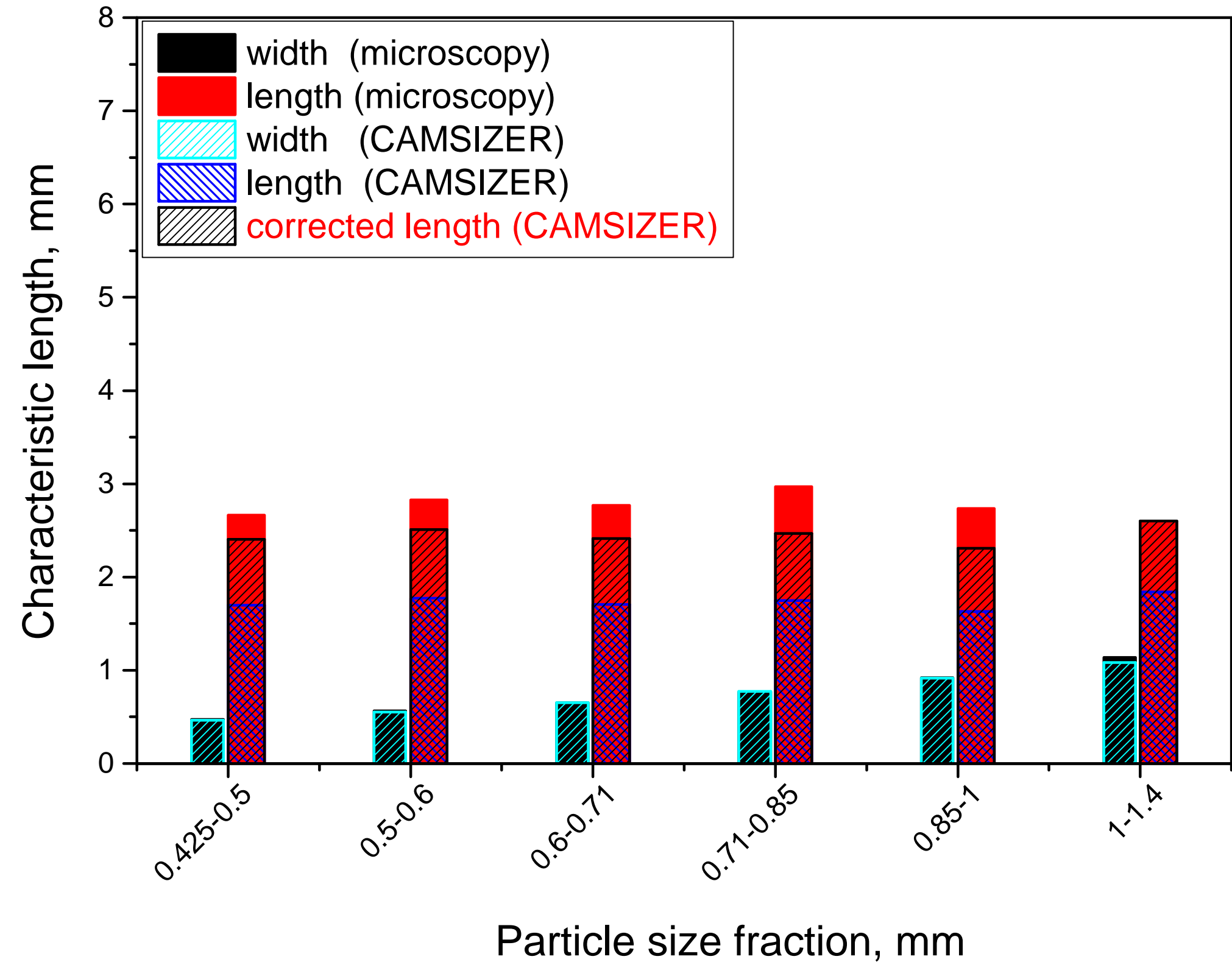
- 1
2
3
4
5
6
7
8
9
10 514 particle size analysis data obtained from the measurements of non-
11 515 spherical particle systems, *AAPD PharSciTech* 7 (3) (2006) 93–106.
- 12
13
14 516 [33] Matsuyama T, Yamamoto H, Scarlett B, Theoretical prediction of effect
15 517 of orientation on diffraction pattern transformation of diffraction pattern
16 518 due to ellipsoids into equivalent diameter distribution for spheres, *Part*
17 519 *Part Syst Charact* 17 (2000) 41–6.
- 20
21
22 520 [34] Umhauer H, Bottlinger M, Effect of particle shape and structure on
23 521 the results of single particle light-scattering size analysis, *Appl Opt* 30
24 522 (1991) 4980–6.
- 25
26
27
28
29 523 [35] Doroodchi E, Zulfqar H, Moghtaderi B, A combined experimental and
30 524 theoretical study on laboratory-scale comminution of coal and biomass
31 525 blends, *Powder Tech* 235 (2013) 412–21.
- 32
33
34
35 526 [36] Eshel G, Levy GJ, Mingelgrin U, Singer MJ, Critical Evaluation of the
36 527 Use of Laser Diffraction for Particle-Size Distribution Analysis, *Soil Sci*
37 528 *Soc Am J* 68 (2004) 736–43.
- 38
39
40
41
42 529 [37] Cardoso CR, Oliveira TJP, Santana Junior JA, Ataide CH, Physical
43 530 characterization of sweet sorghum bagasse, tobacco residue, soy hull
44 531 and fiber sorghum bagasse particles: Density, particle size and shape
45 532 distributions, *Powder Tech* 245 (2013) 105–14.
- 46
47
48
49
50 533 [38] Igathinathane C, Pordesimo LO, Columbus EP, Batchelor WD,
51 534 Methuku SR, Shape identification and particle size distribution from
52 535 basic shape parameters using ImageJ, *Comp Electr Agricult* 63 (2008)
53 536 168–82.

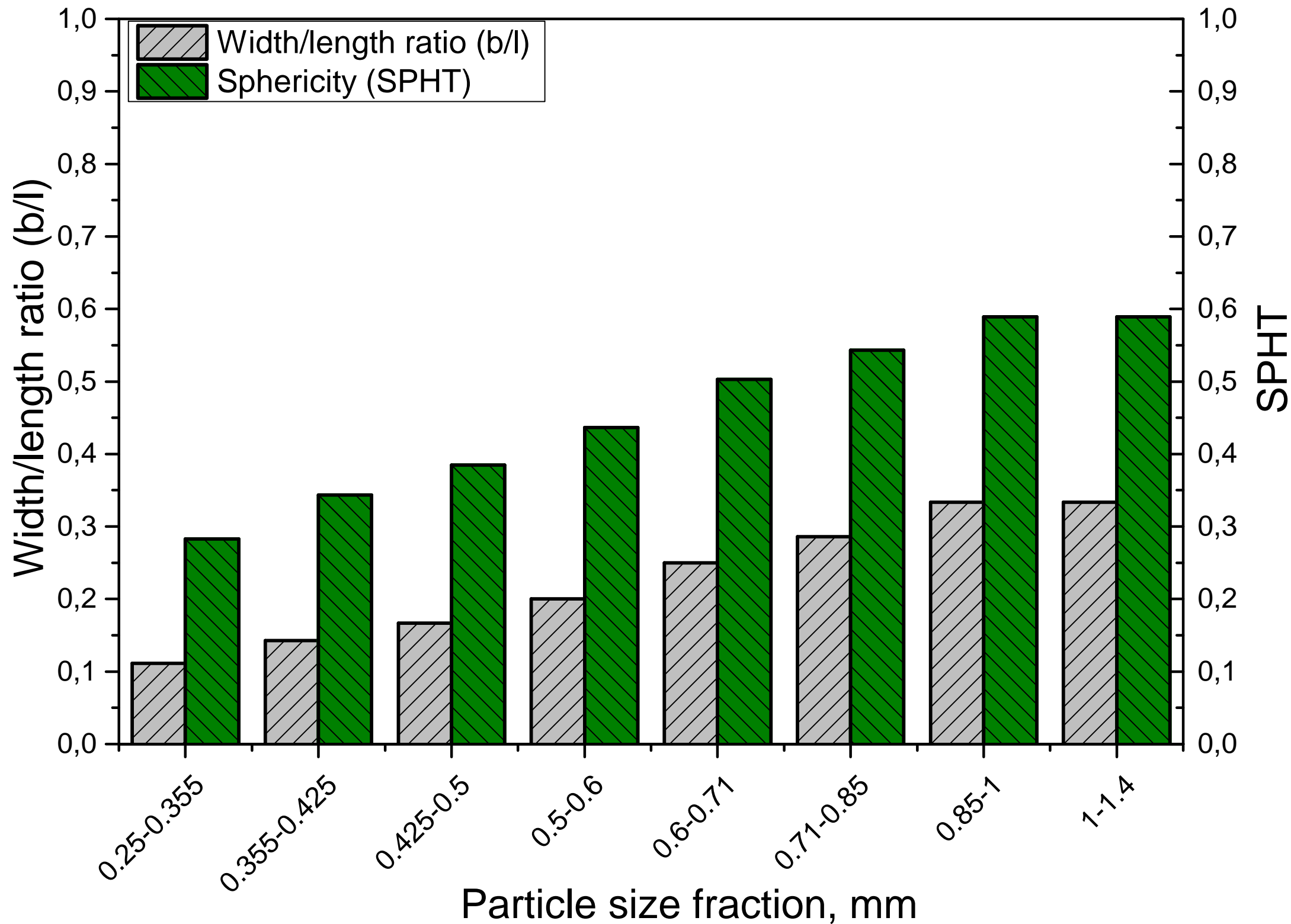
- 1
2
3
4
5
6
7
8
9
10 537 [39] Geimer RL, Evans JW, Setiabudi D, Flake Furnish Characterization:
11 538 Modeling Board Properties with Geometric Descriptors, Forest Prod
12
13 539 Lab, 1999.
- 14
15
16 540 [40] Momeni M, Fundamental Study of Single Biomass Particle Combustion.
17
18 541 PhD thesis, Aalborg University (2012).
- 19
20
21 542 [41] Trubetskaya A, Surup G, Shapiro A, Bates RB, Modeling the influence of
22
23 543 potassium content and heating rate on biomass pyrolysis, Appl Energy
24
25 544 194 (2017) 199–211.
- 26
27 545 [42] Bellais M, Modelling of the pyrolysis of large wood particles. PhD thesis,
28
29 546 KTH Royal Institute of Technology (2007).
- 30
31
32 547 [43] Grønli MG, A Theoretical and Experimental Study of the Thermal
33
34 548 Degradation of Biomass. PhD thesis, Norwegian University of Science
35
36 549 and Technology (1996).
- 37
38
39 550 [44] Momeni M, Yin C, Køer SK, Hansen TB, Jensen PA, Glarborg P, Exper-
40
41 551 imental Study on Effects of Particle Shape and Operating Conditions on
42
43 552 Combustion Characteristics of Single Biomass Particles, Energy Fuels 27
44
45 553 (2012) 507–14.
- 46
47 554 [45] Grammelis P, Solid Biofuels for Energy. A Lower Greenhouse Gas Al-
48
49 555 ternative, Springer, 2011.
- 50
51
52 556 [46] Lu H, Experimental and modeling investigations of biomass particle
53
54 557 combustion. PhD thesis, Brigham Young University (2006).
- 55
56
57
58
59
60
61
62
63
64
65

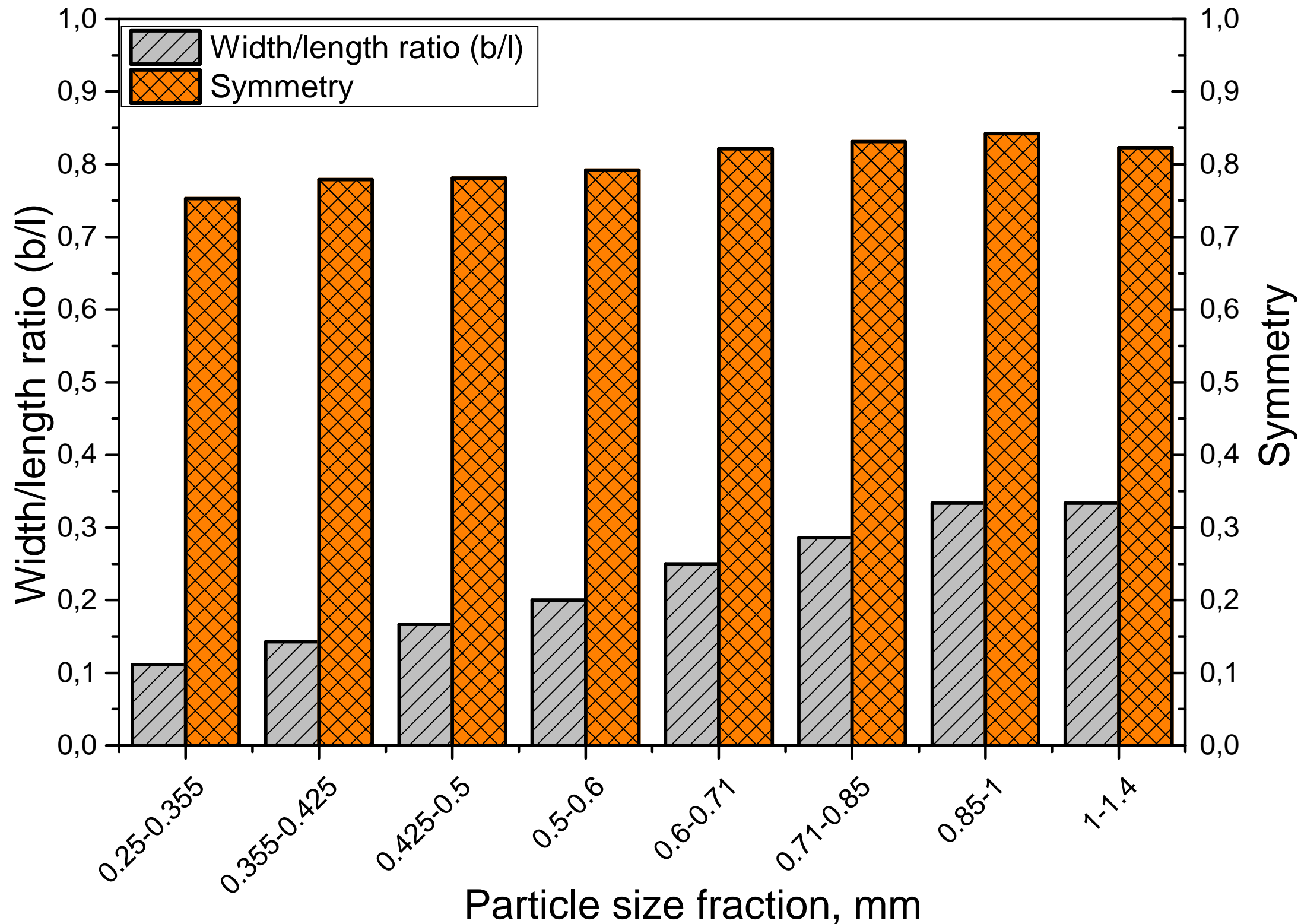
1
2
3
4
5
6
7
8
9
10
11
12
13
14
15
16
17
18
19
20
21
22
23
24
25
26
27
28
29
30
31
32
33
34
35
36
37
38
39
40
41
42
43
44
45
46
47
48
49
50
51
52
53
54
55
56
57
58
59
60
61
62
63
64
65

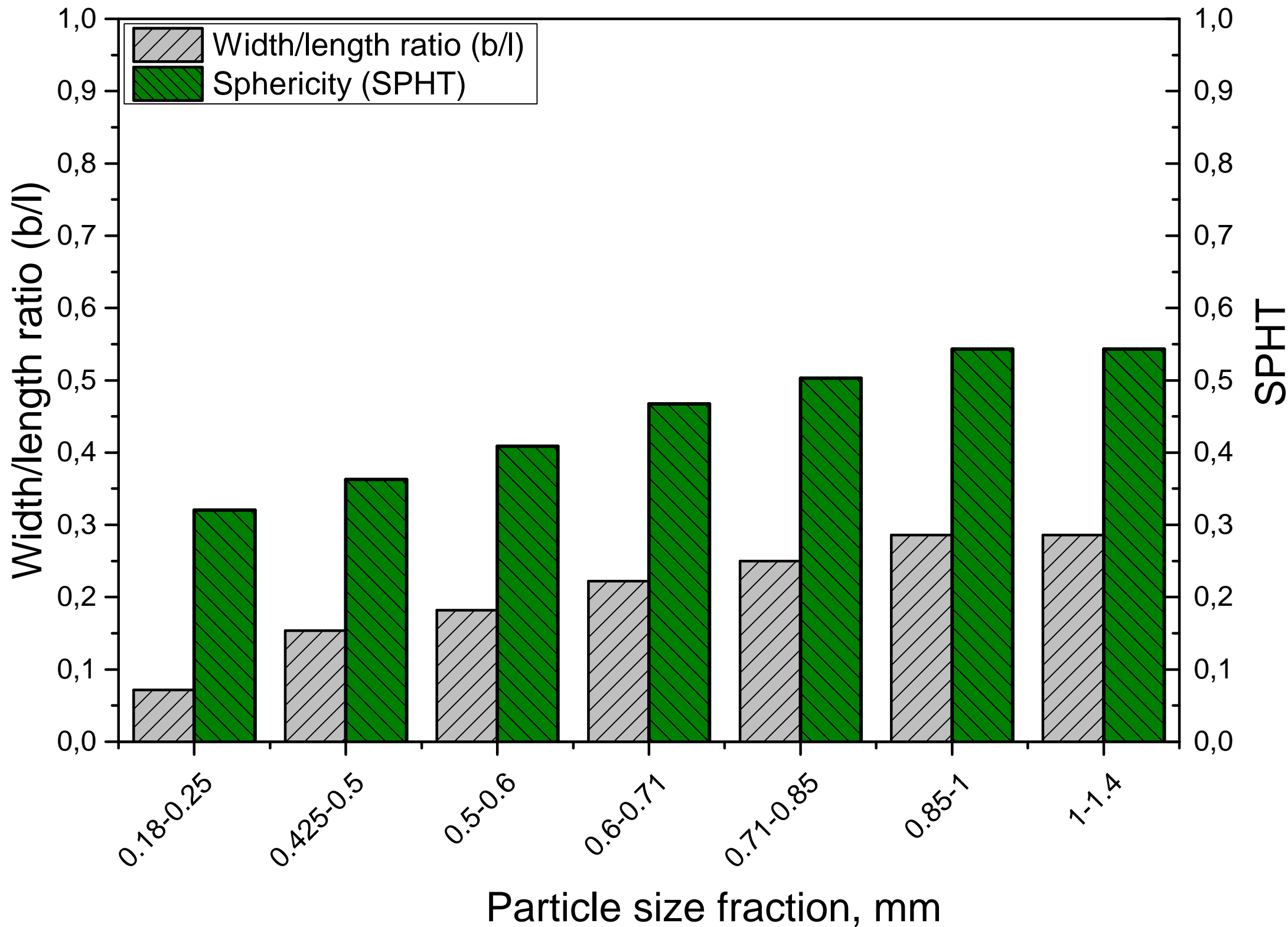
558 [47] Hudson PK, Gibson ER, Young MA, Kleiber PD, Grassian VH, Coupled
559 infrared extinction and size distribution measurements for several clay
560 components of mineral dust aerosol, J Geophys Research 113 (2008)
561 1–11.

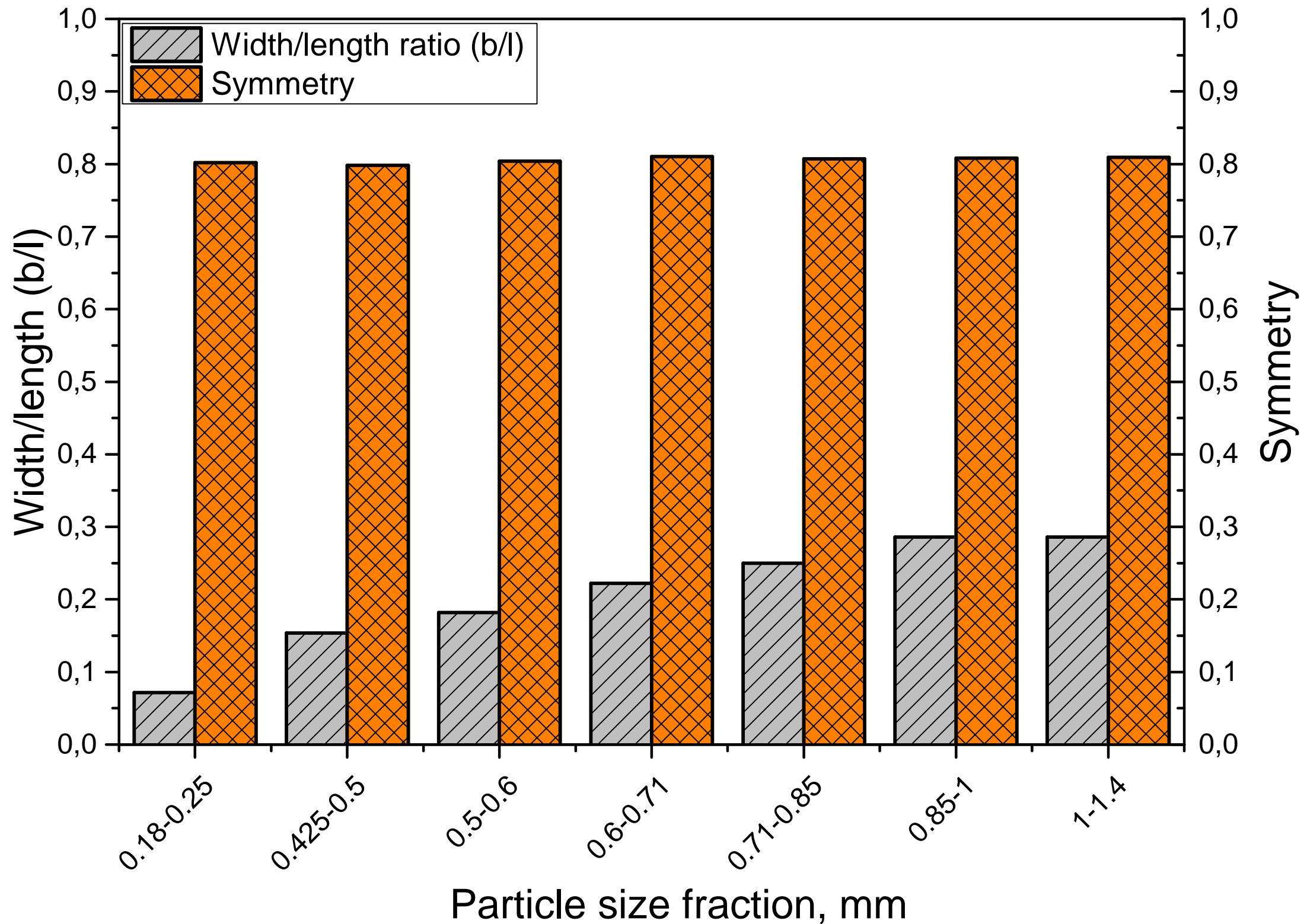


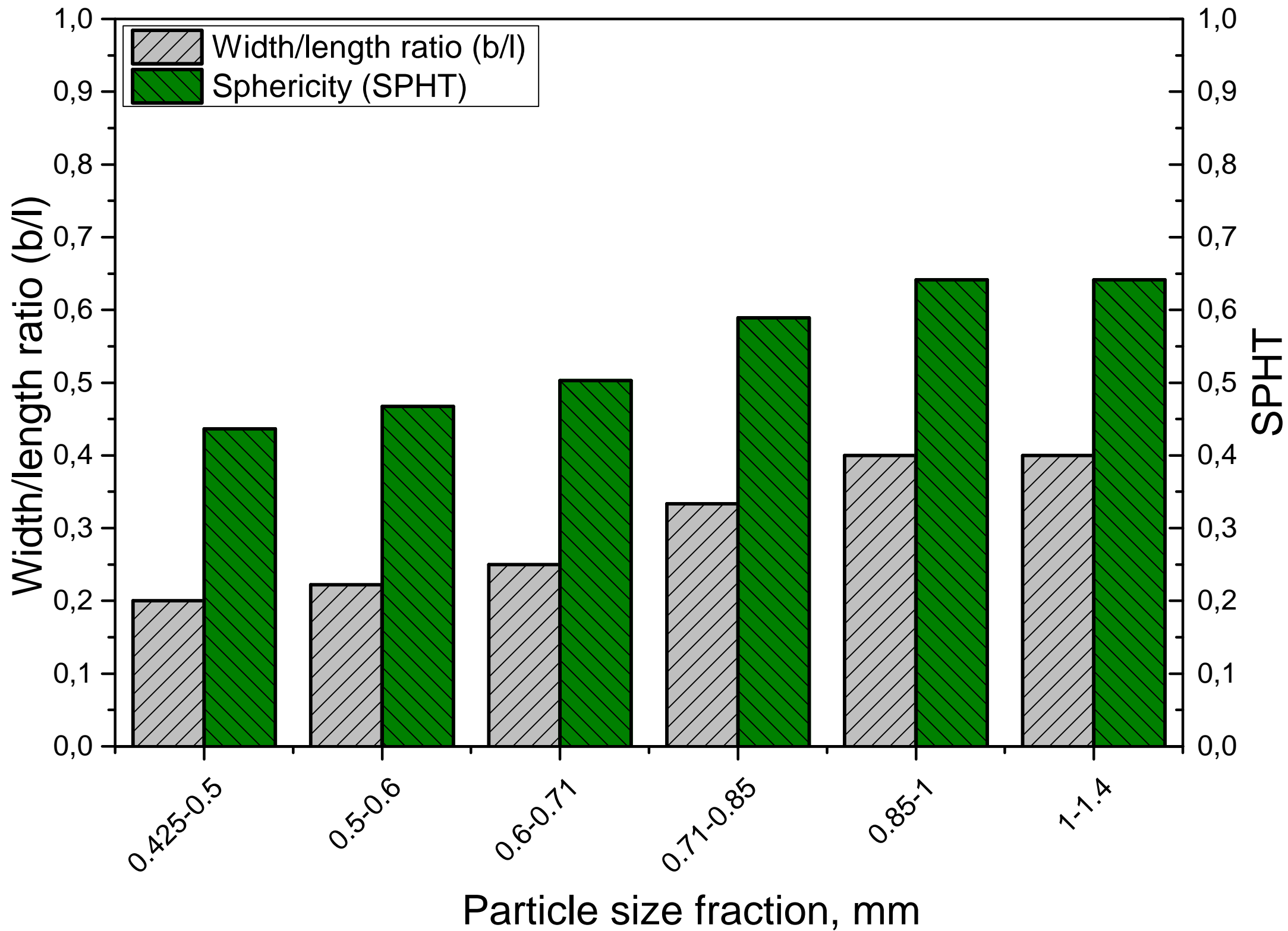


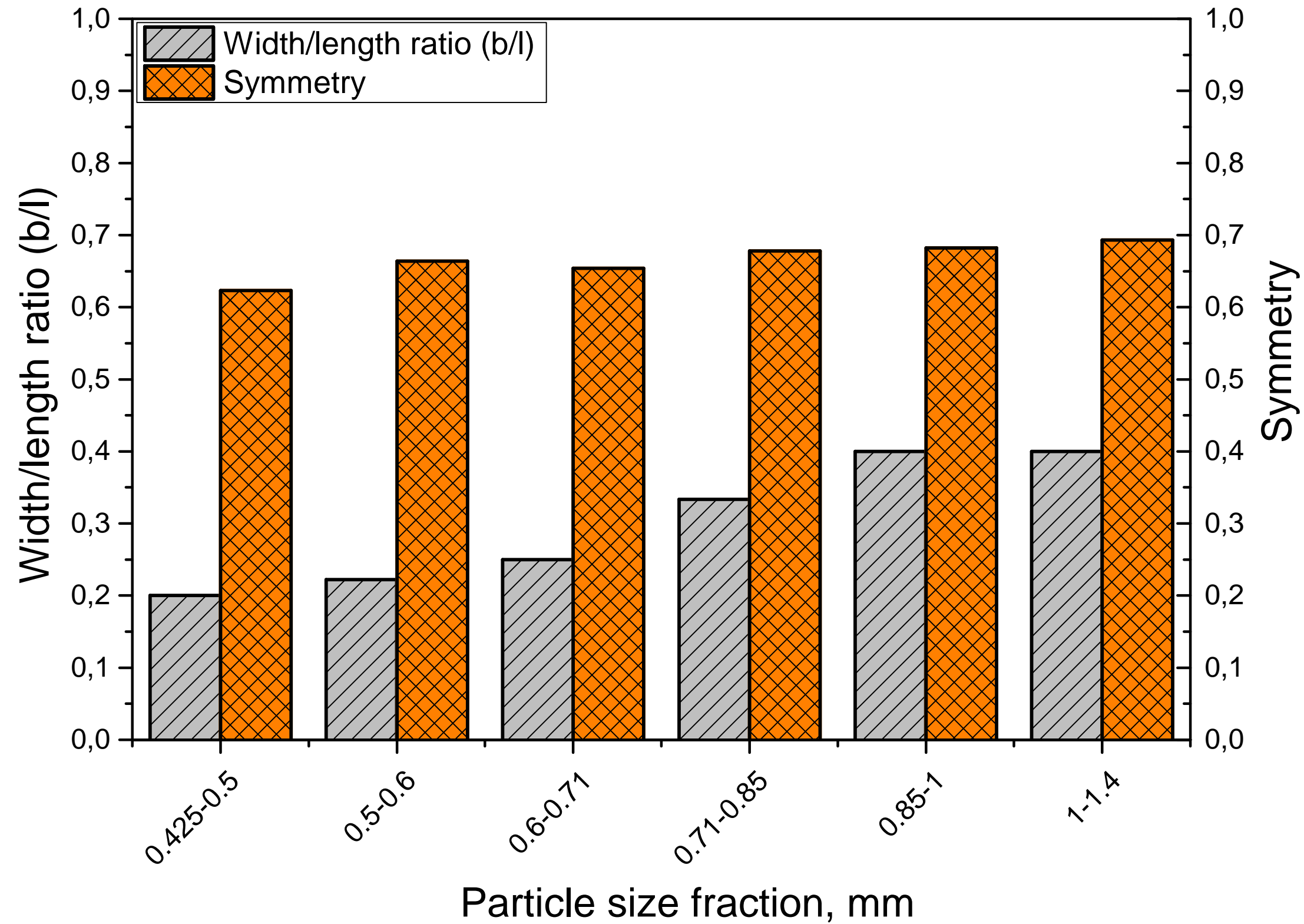


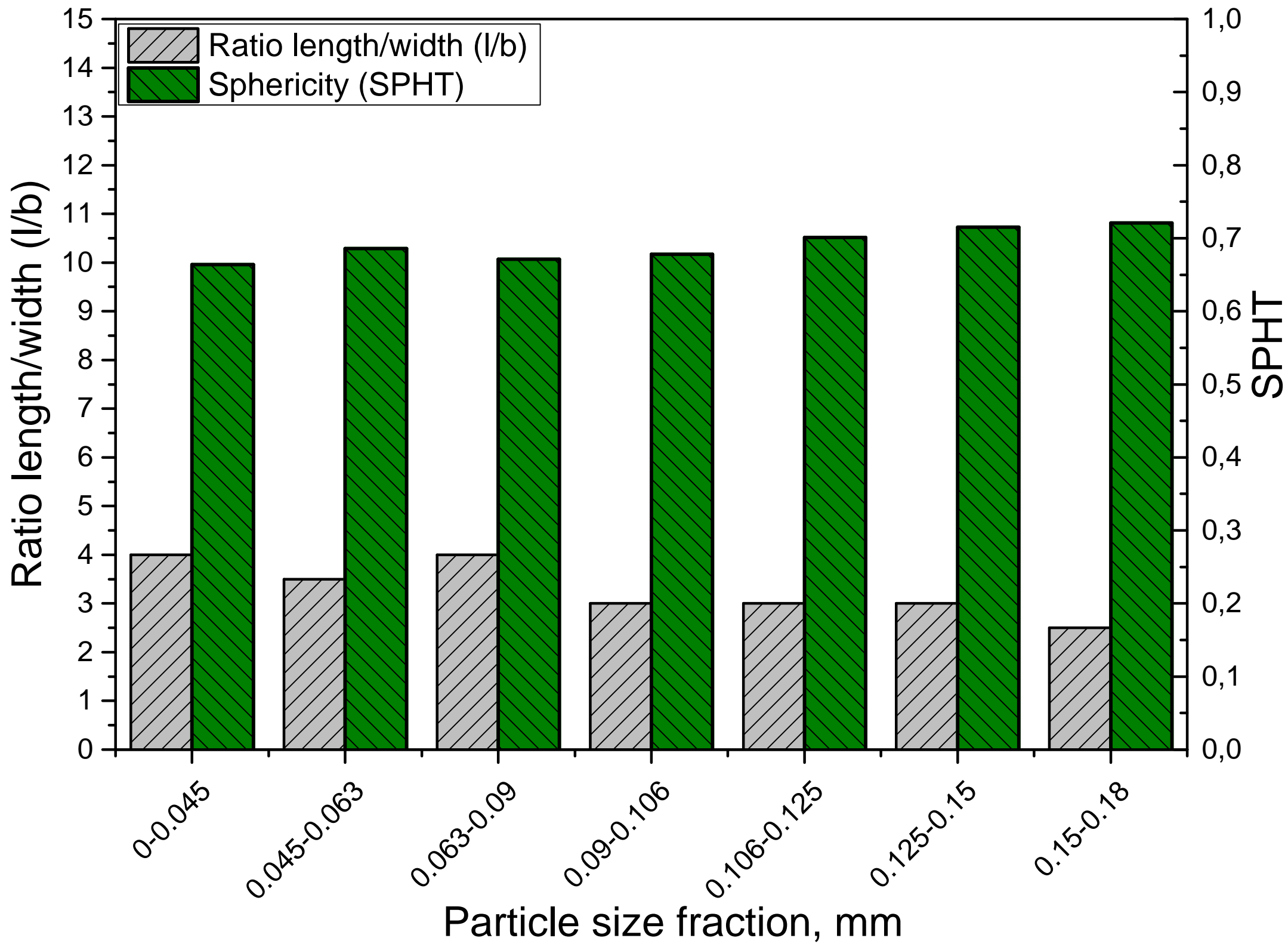


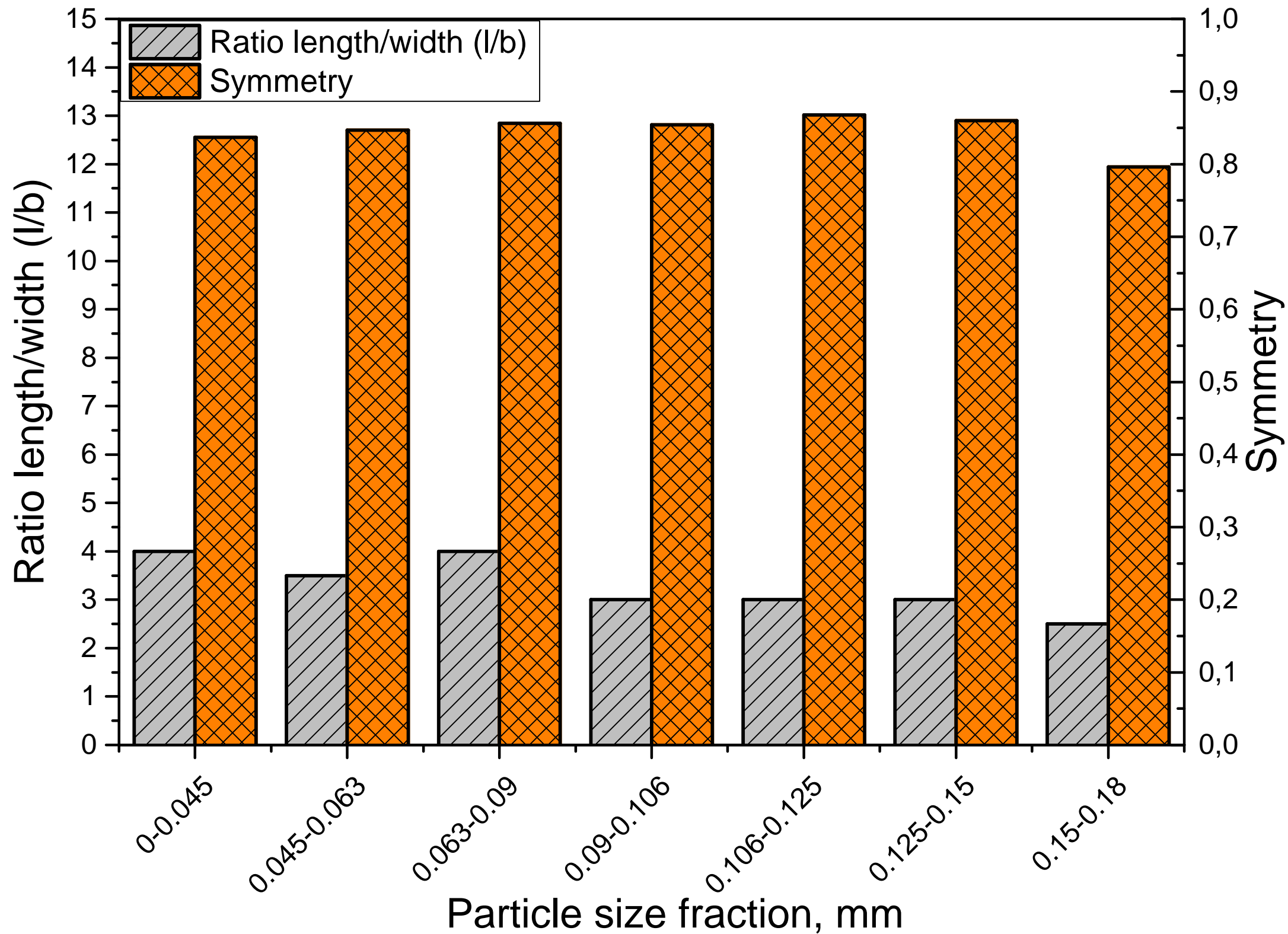


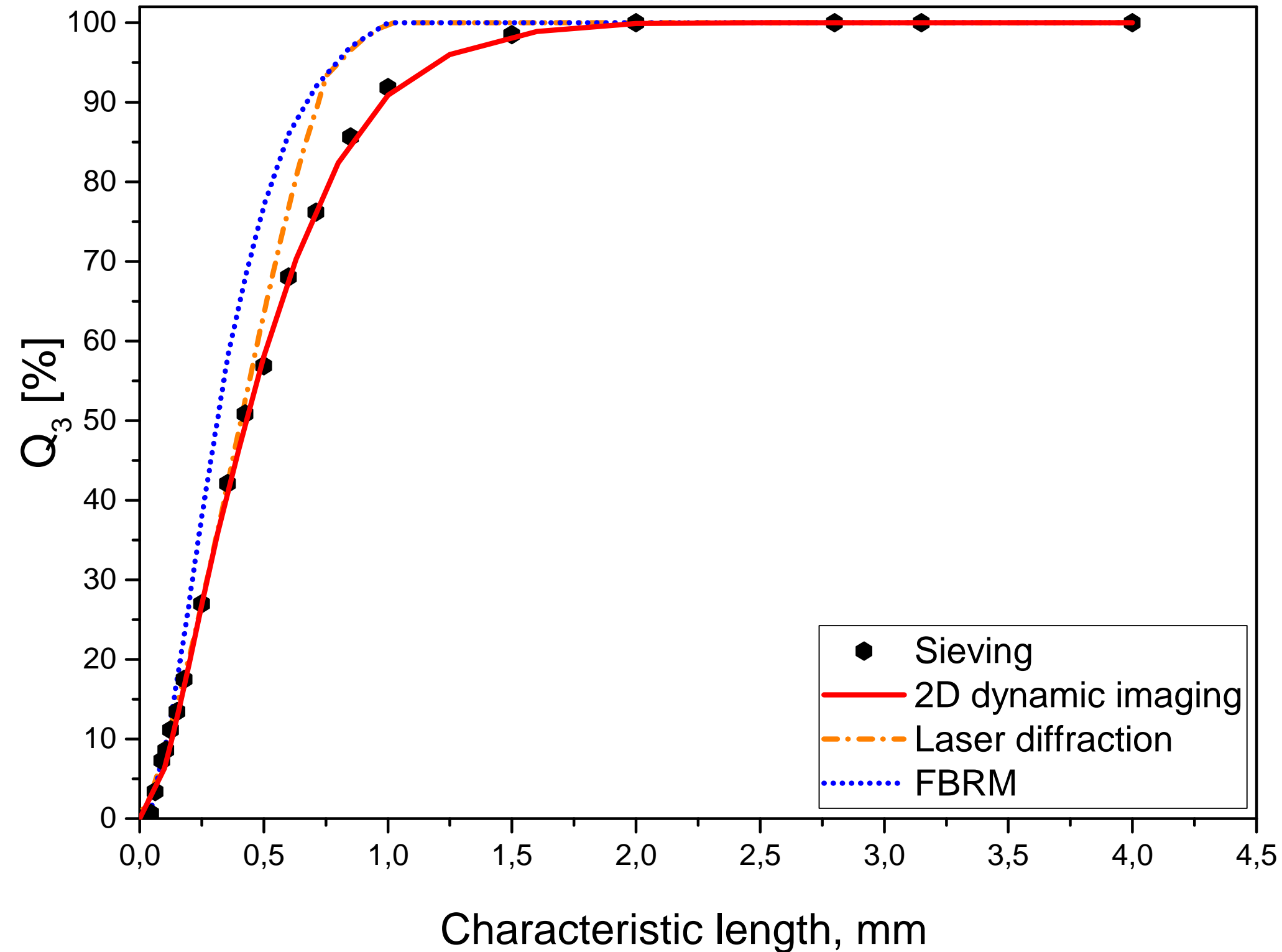


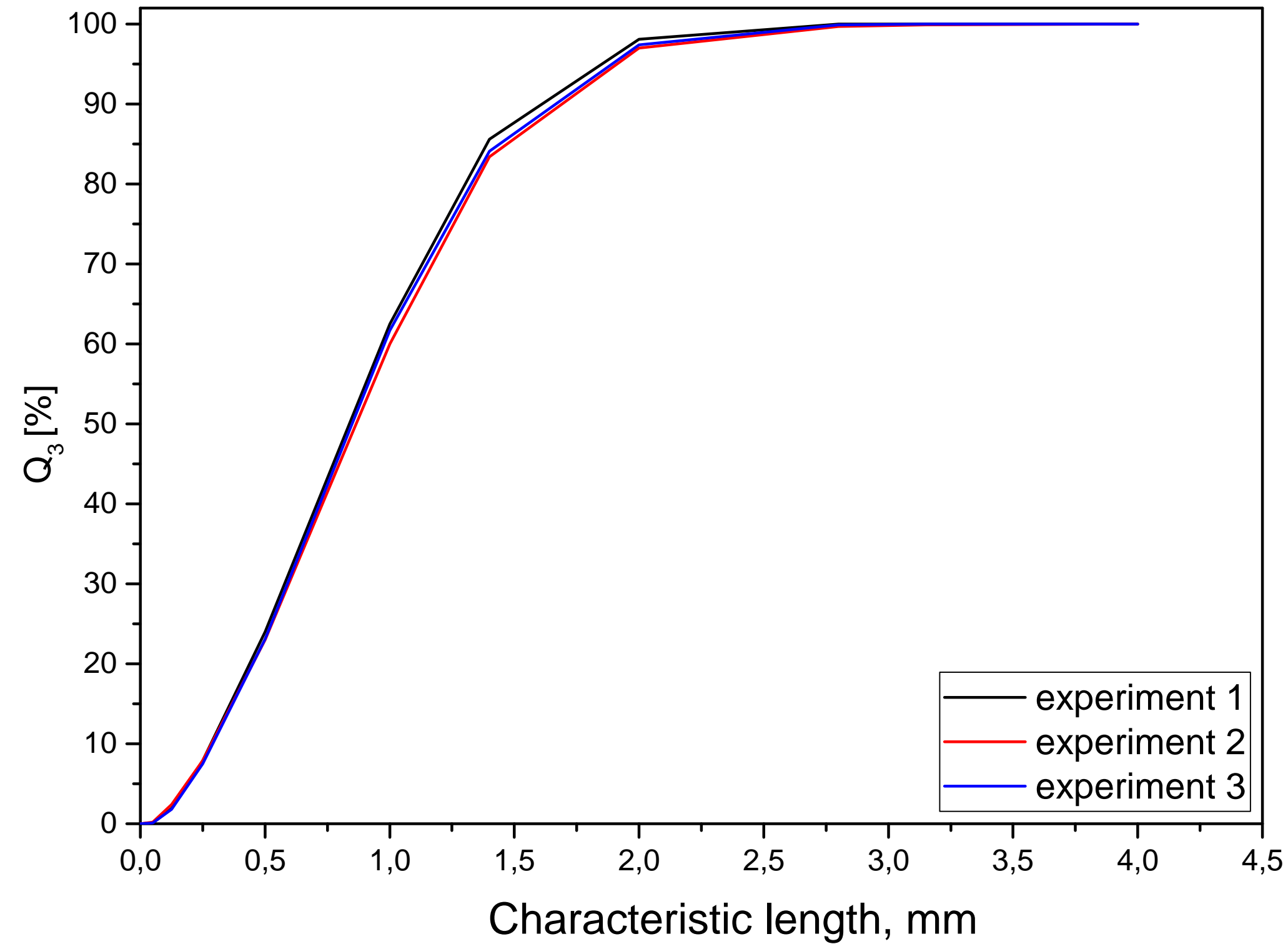


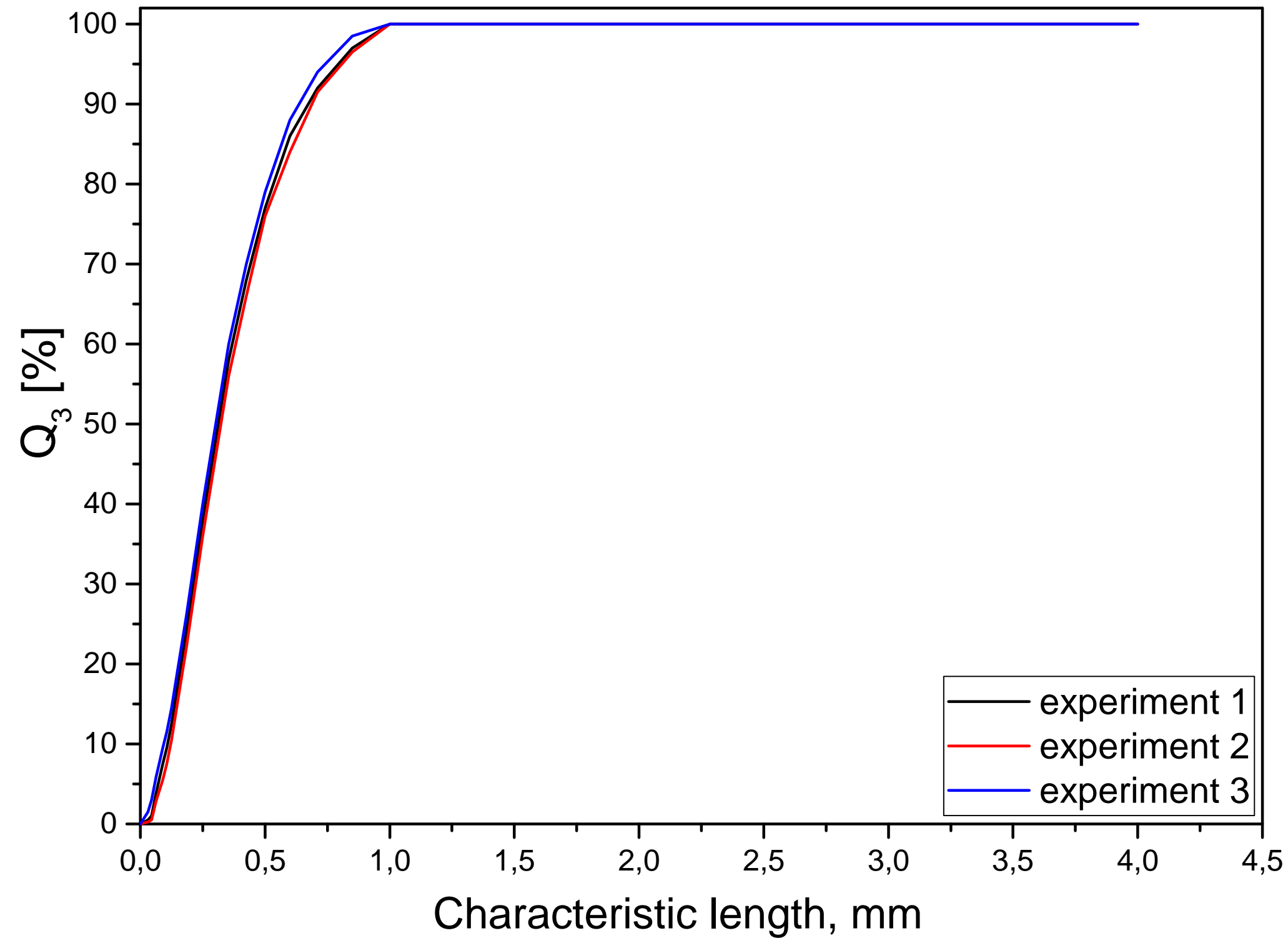


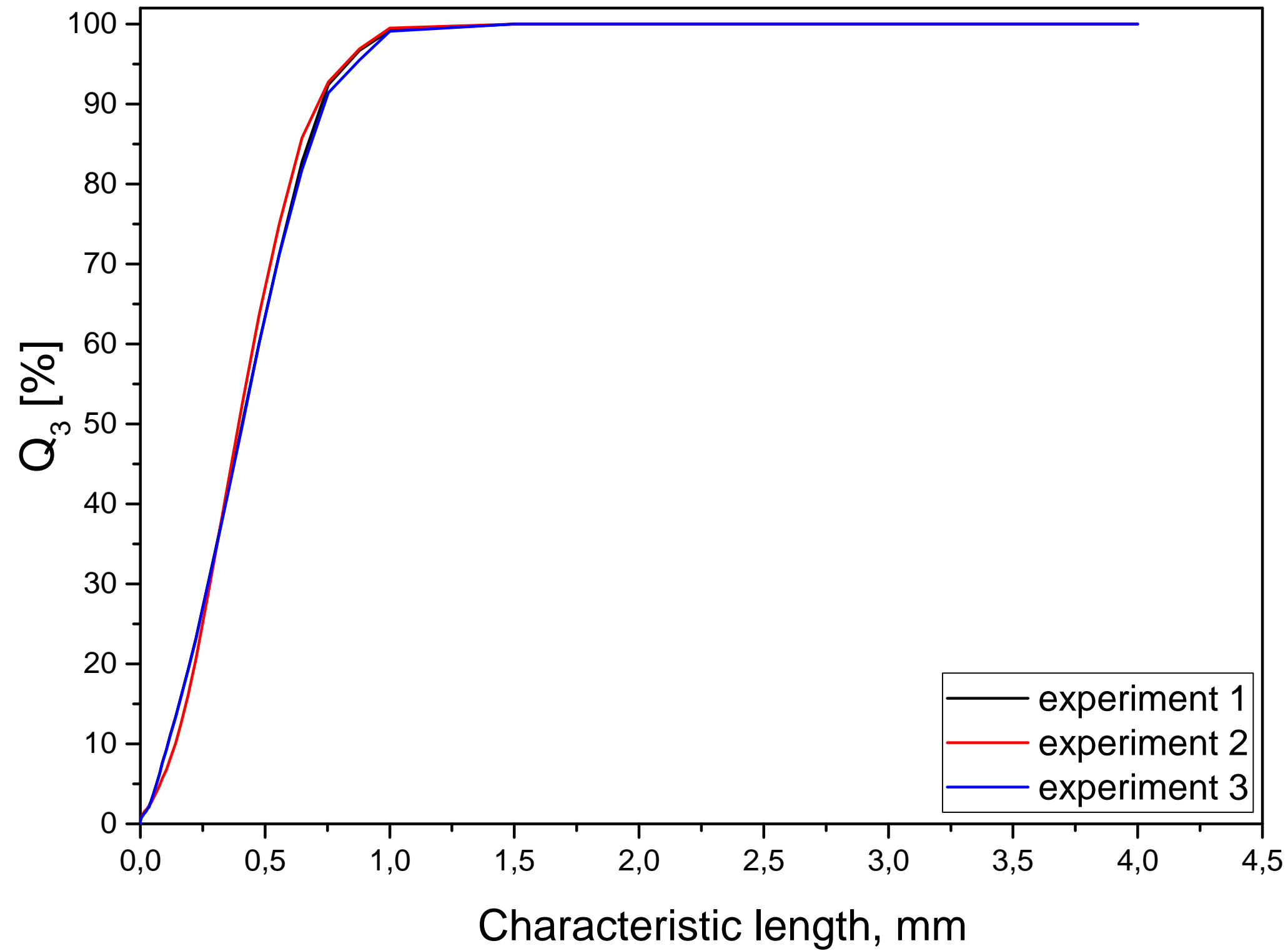


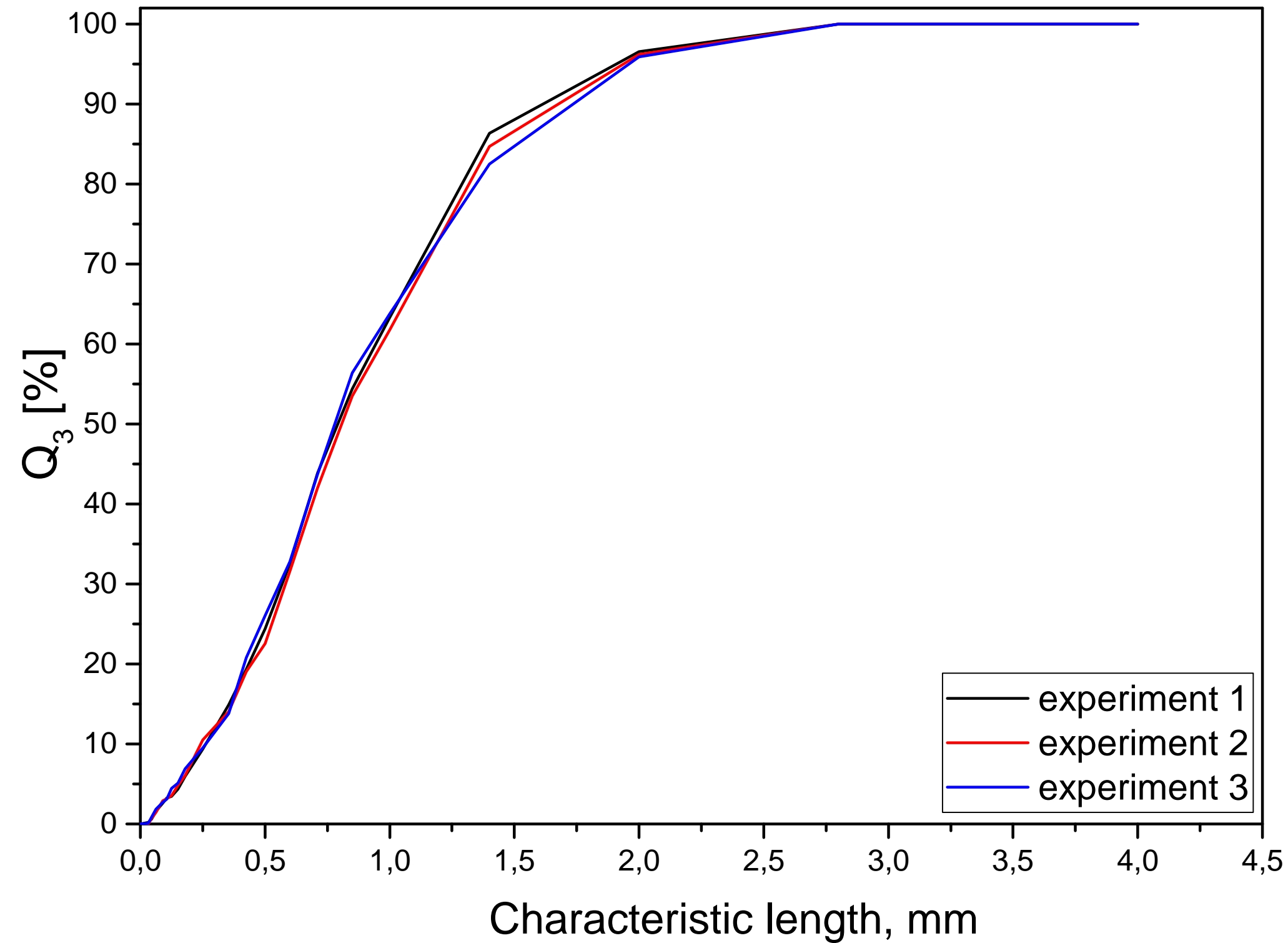


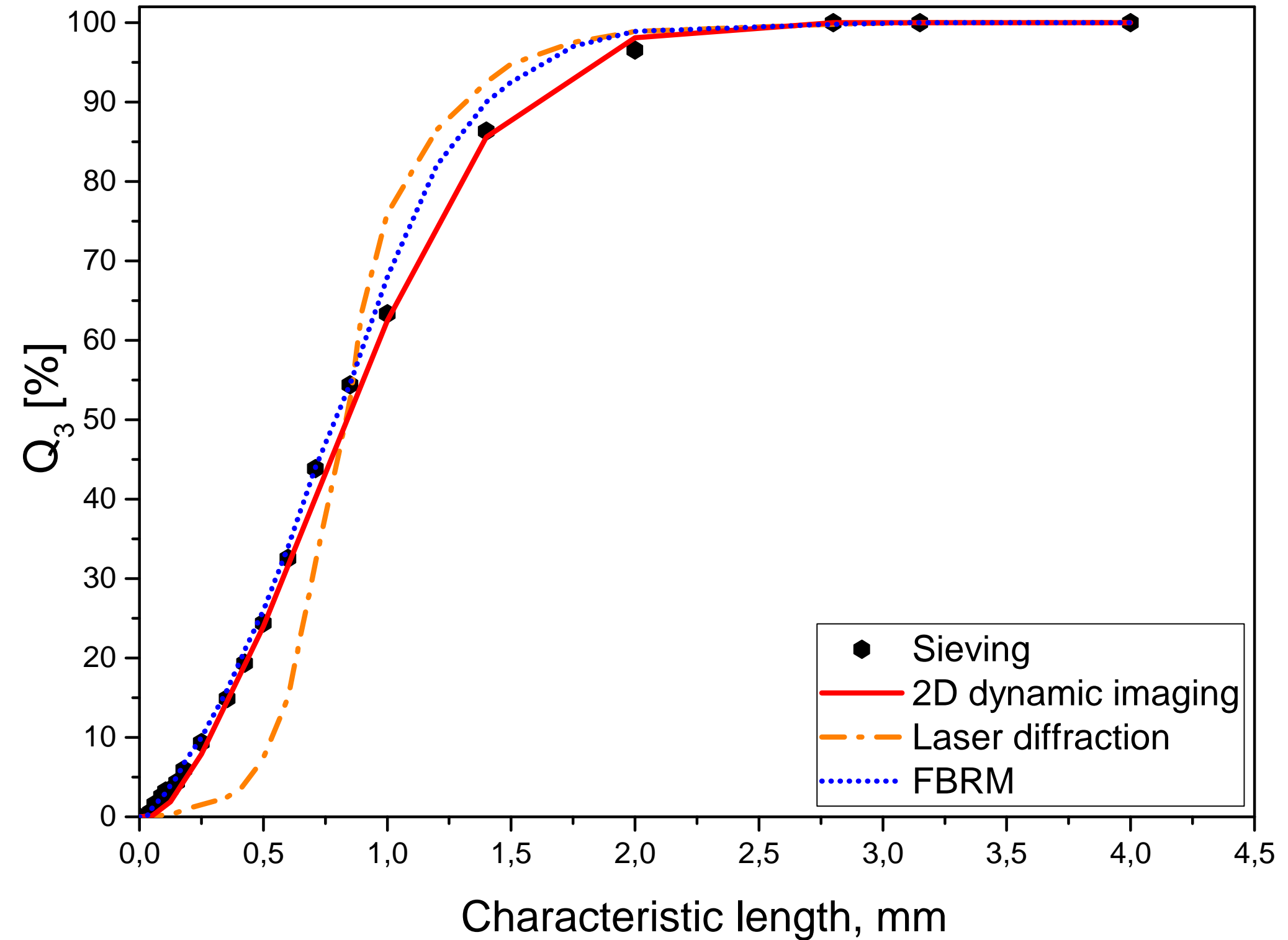


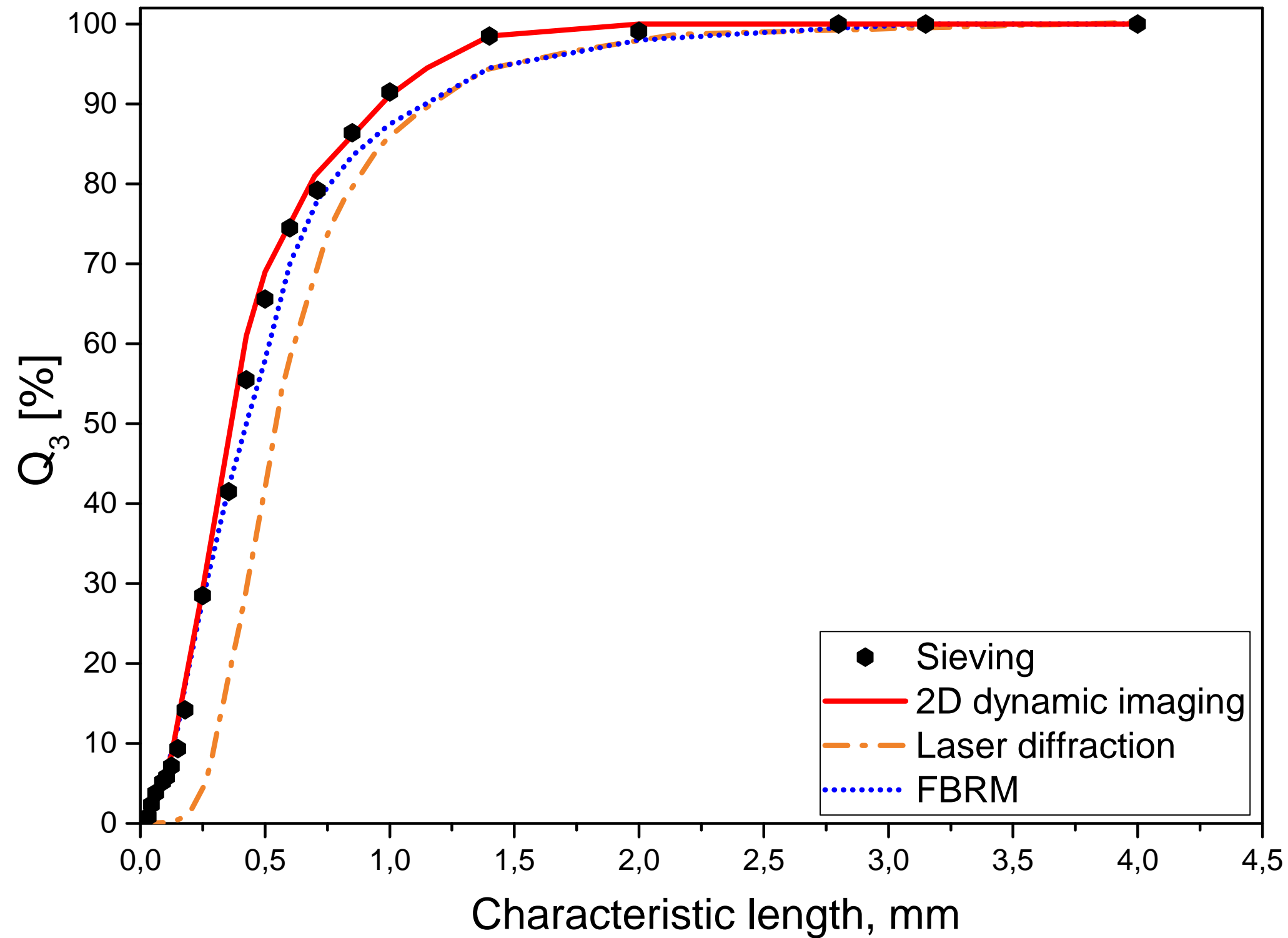












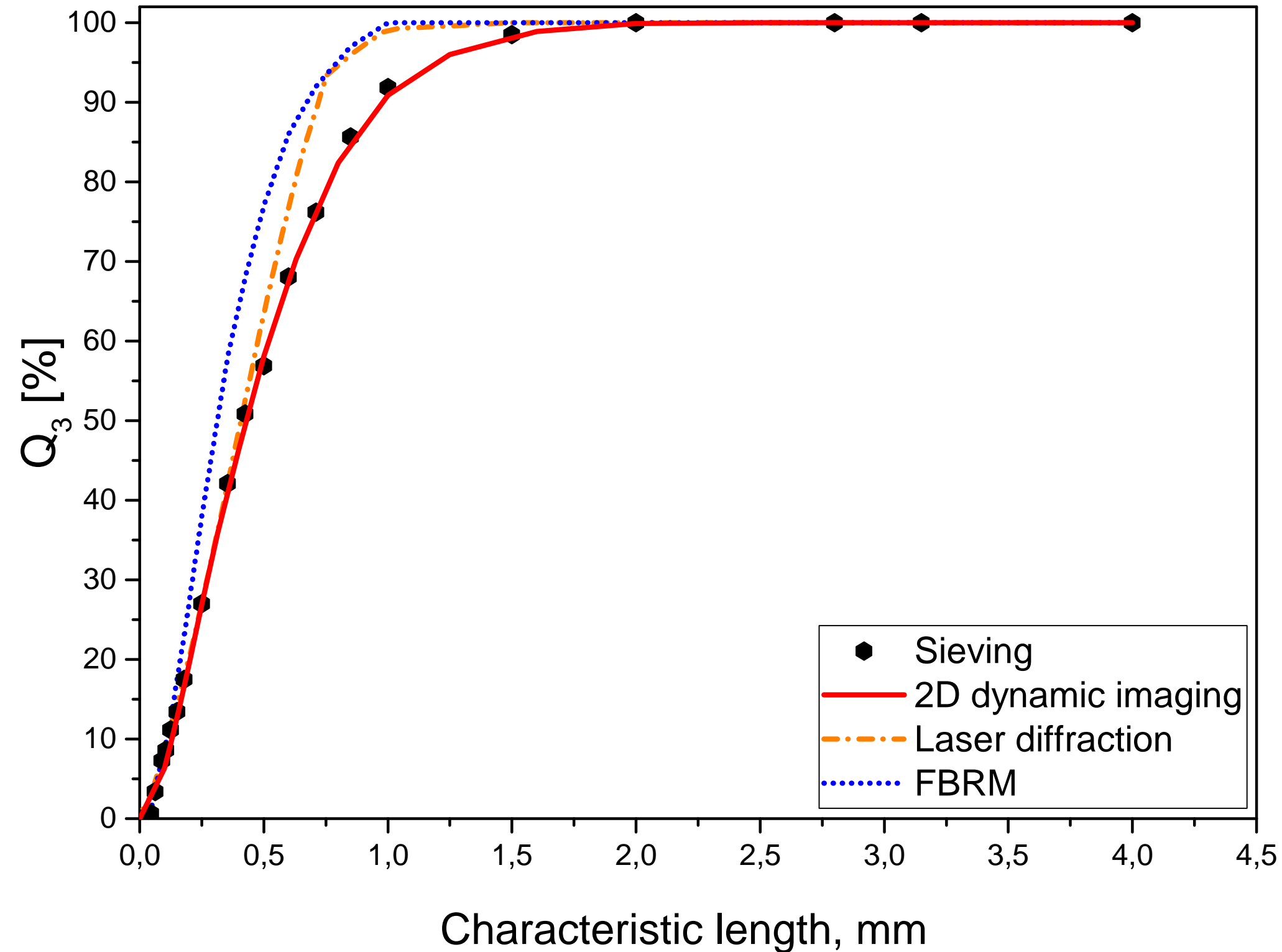
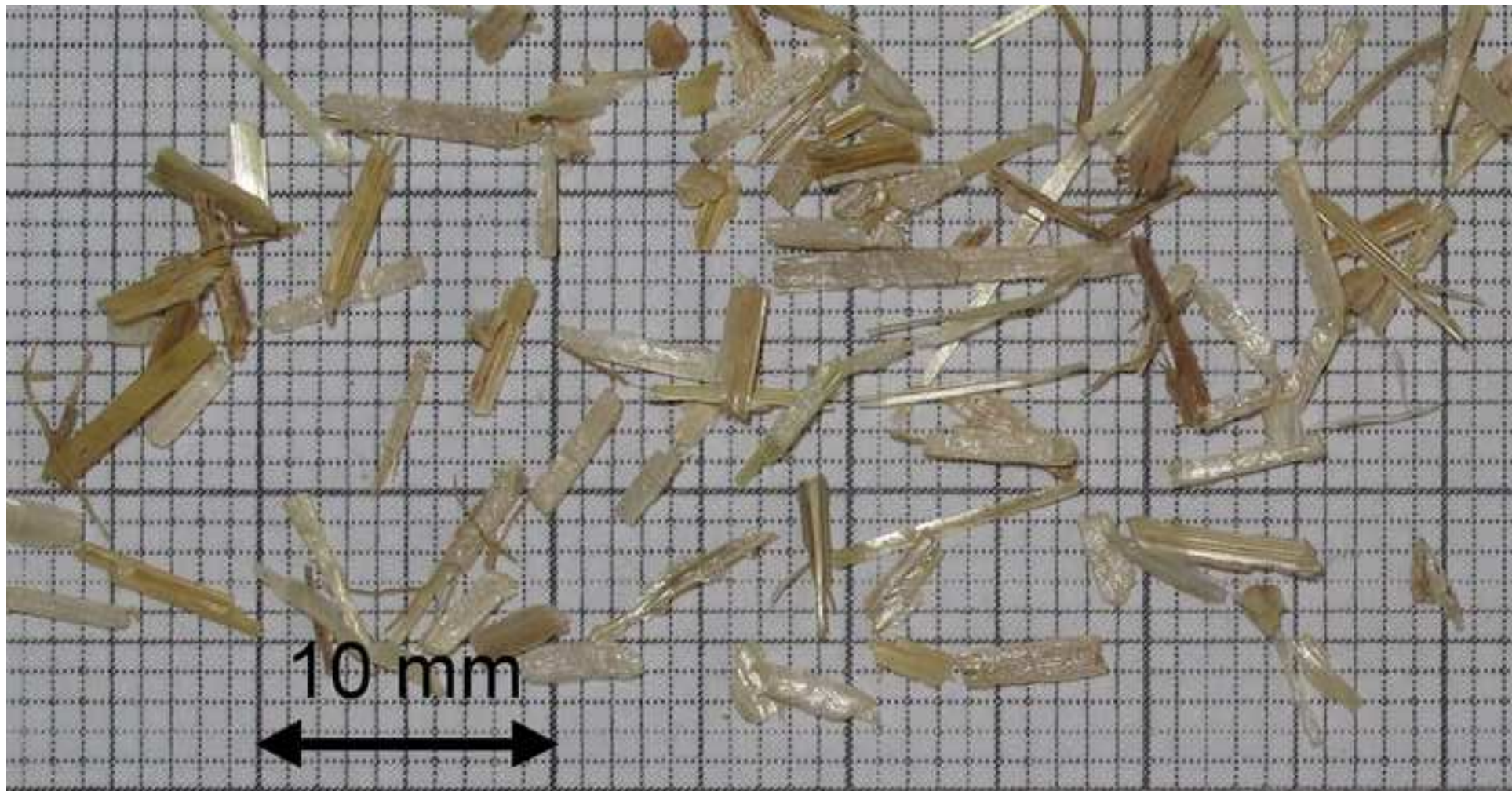
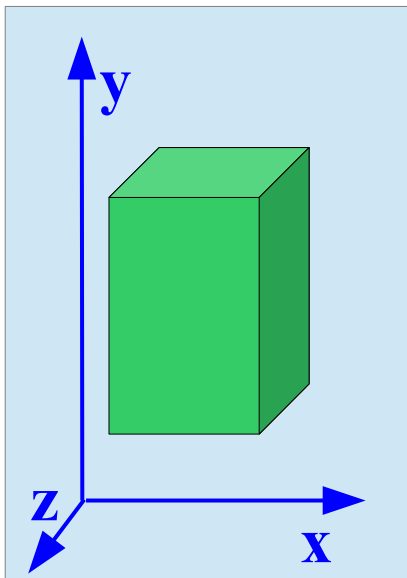


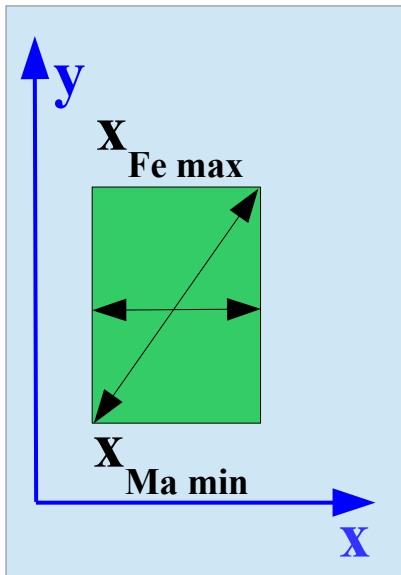
image73.jpg

[Click here to download high resolution image](#)

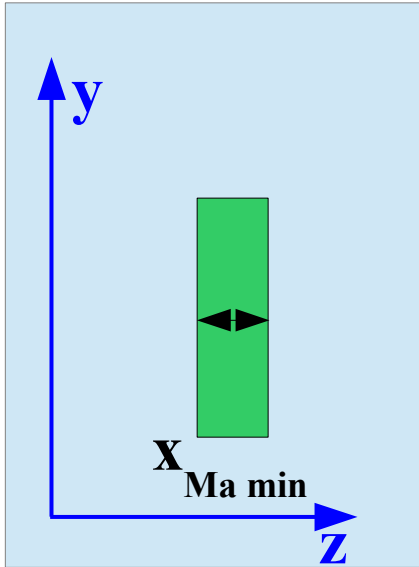


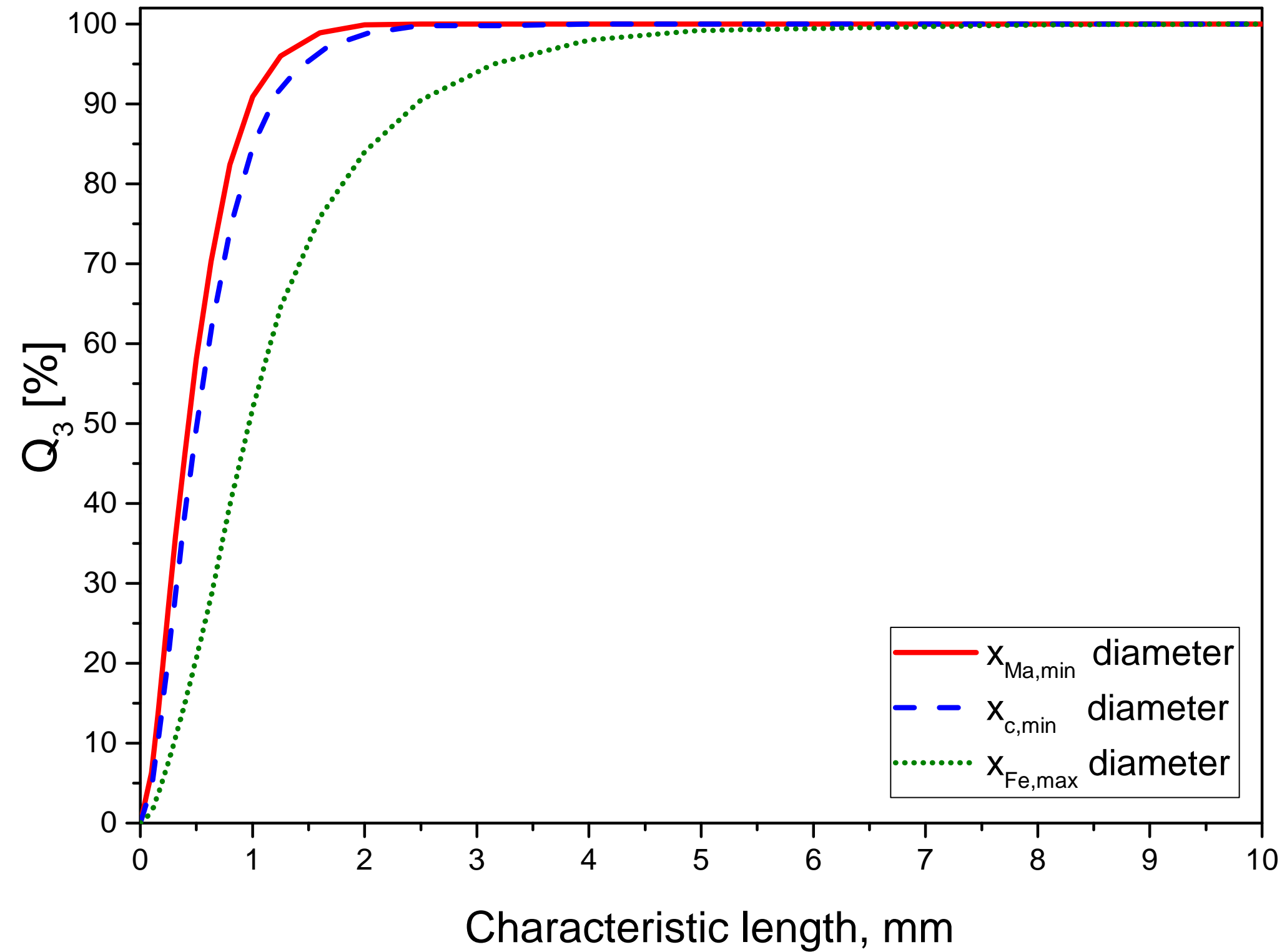


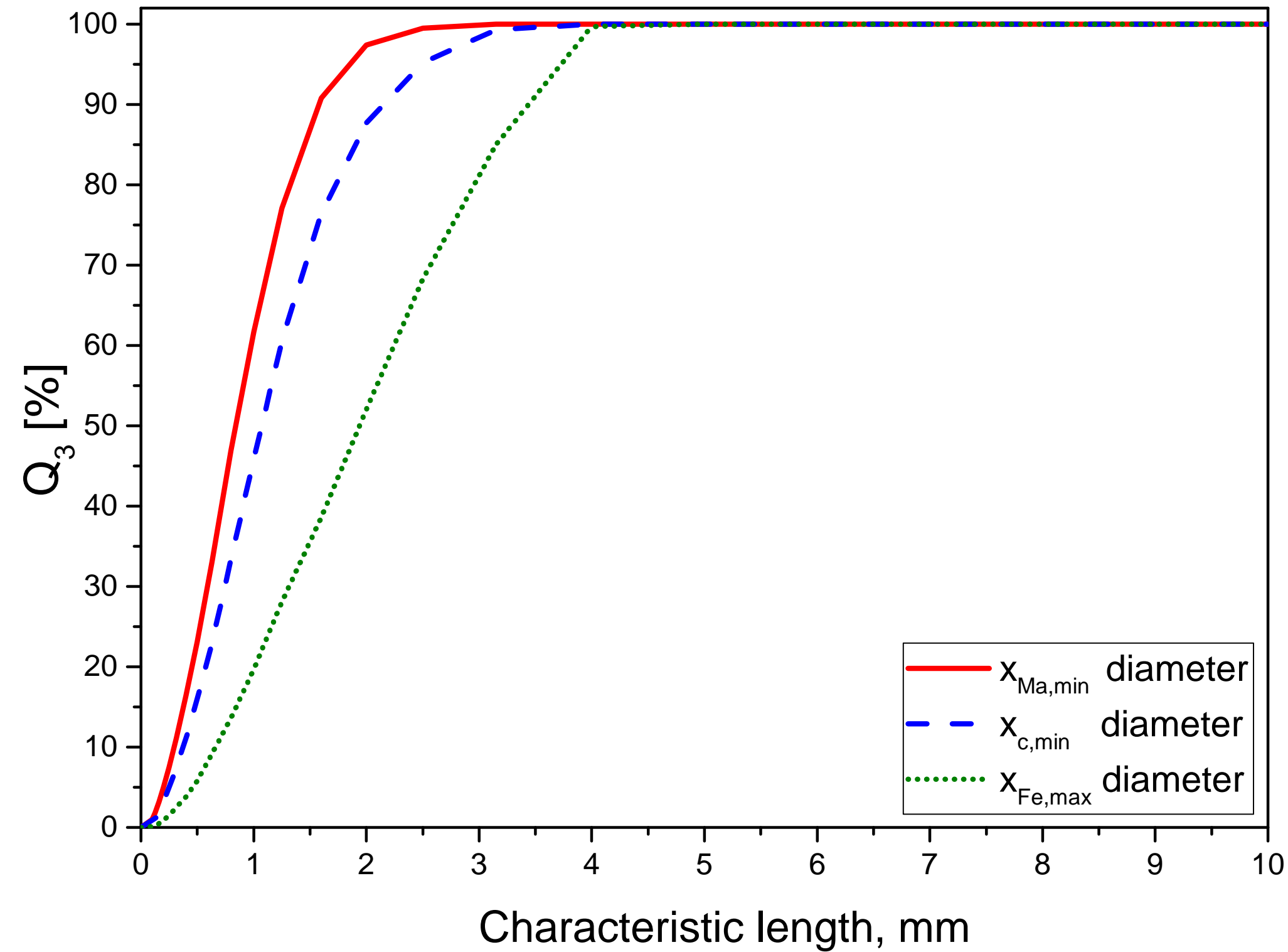


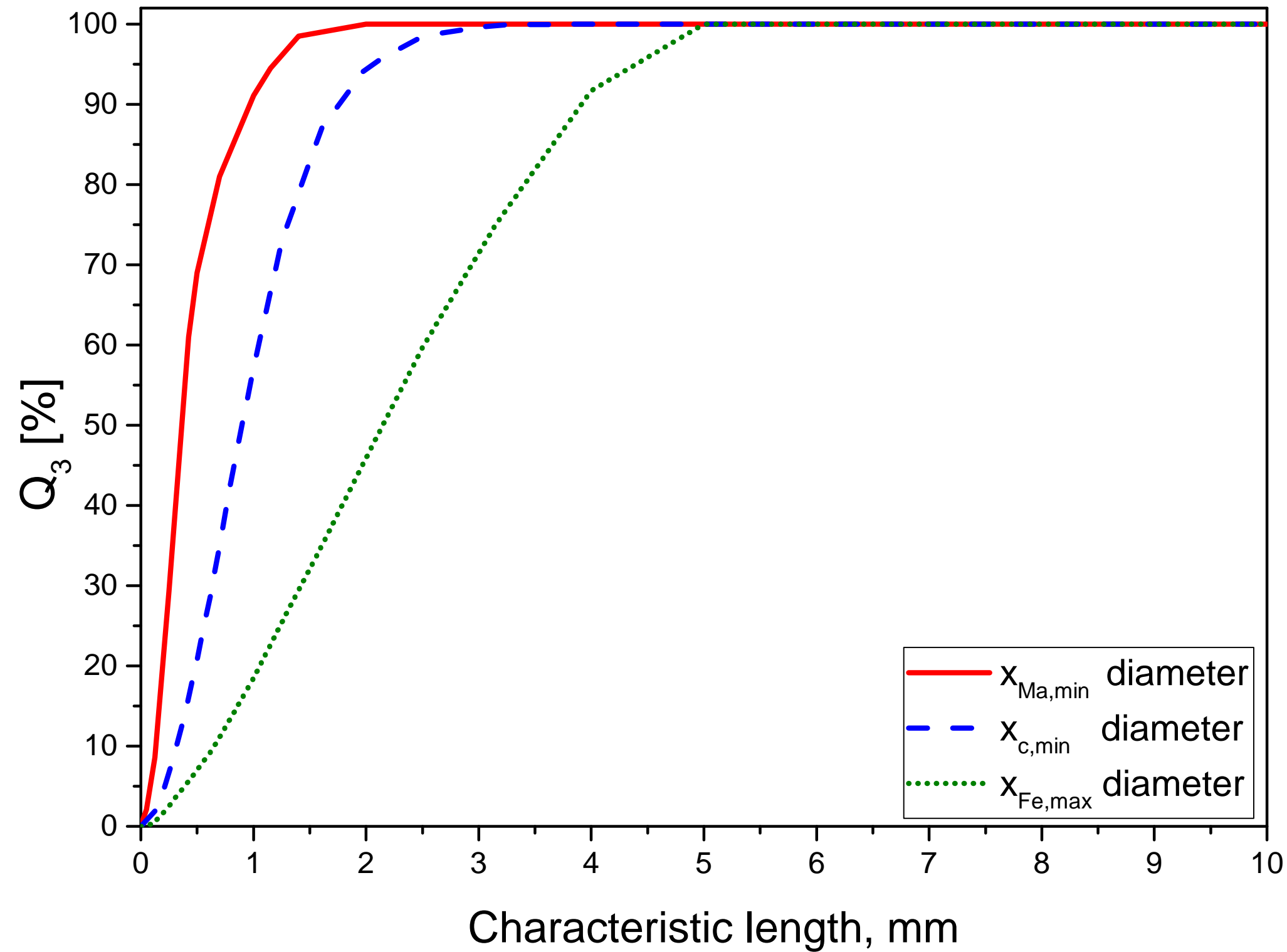


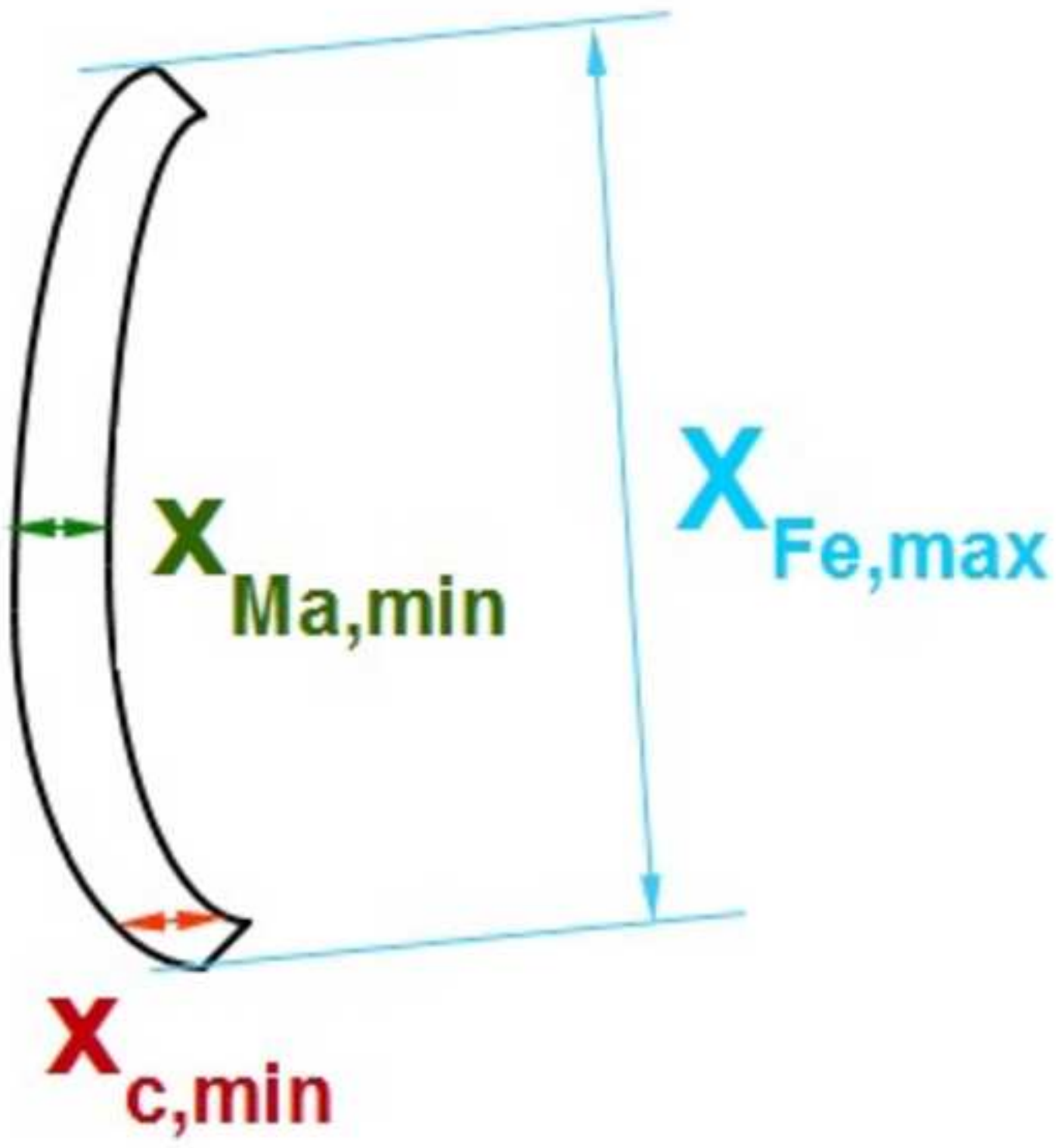












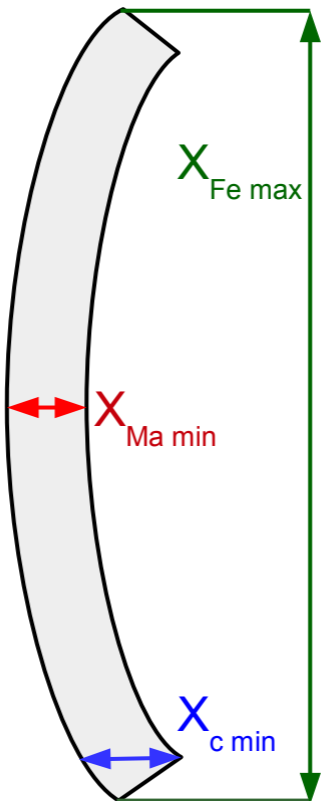
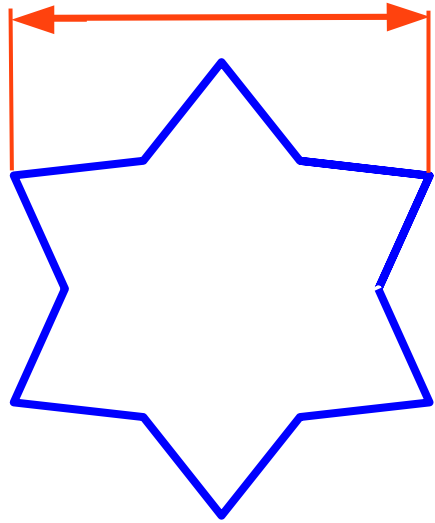
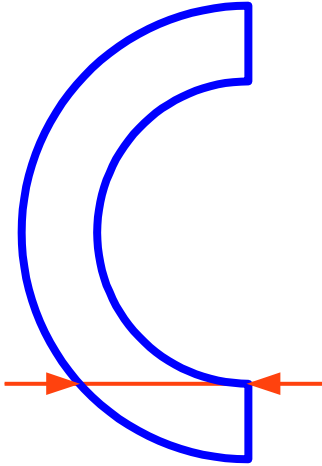
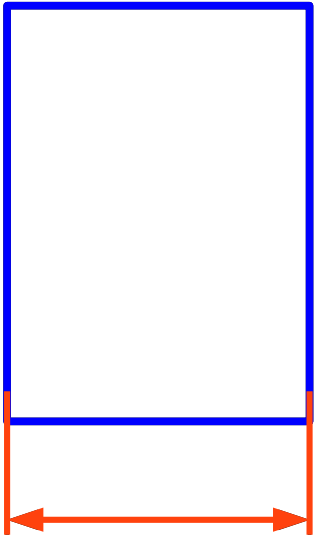
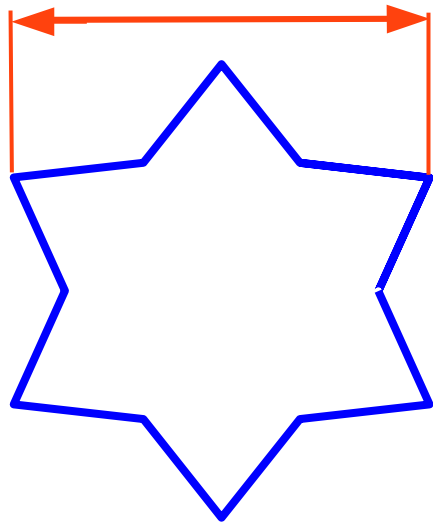
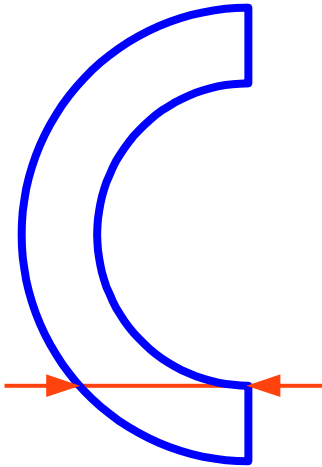
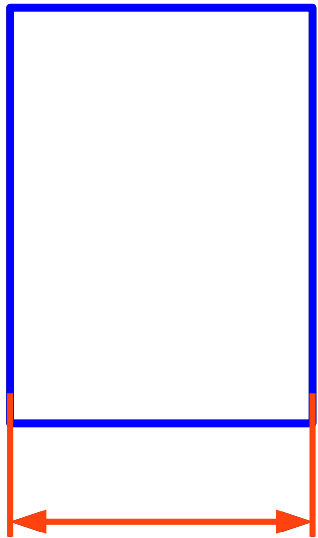
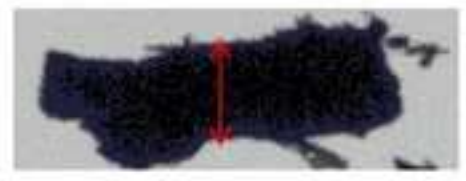
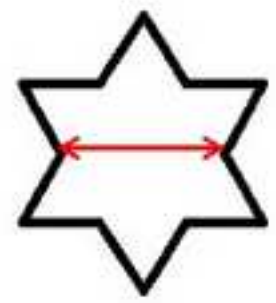
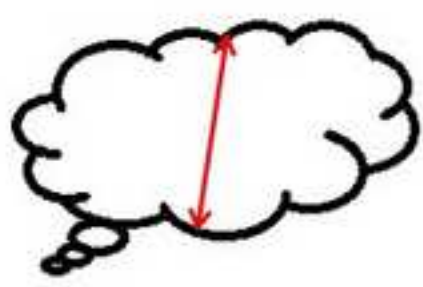
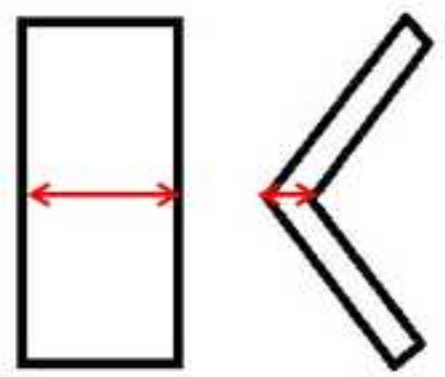
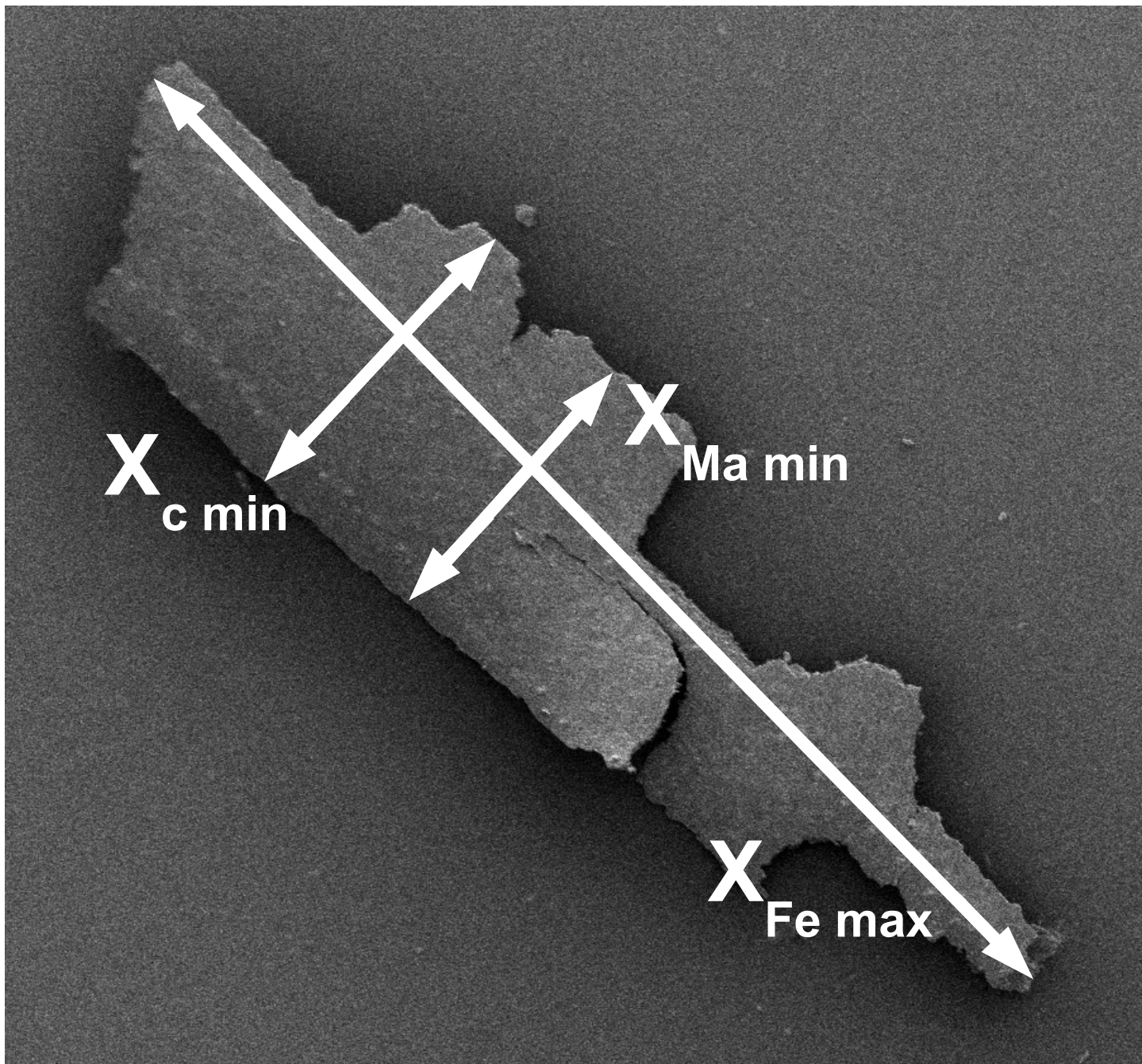


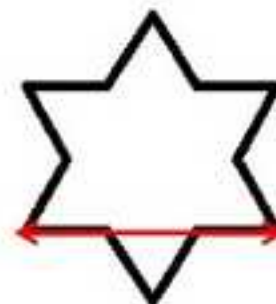
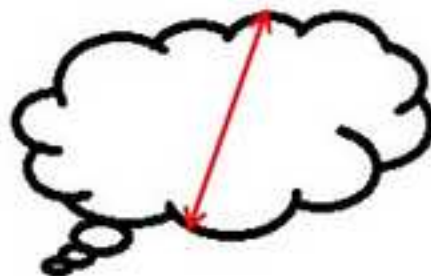
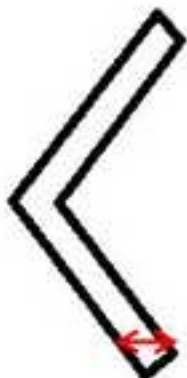
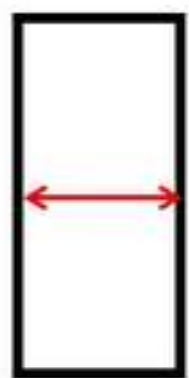
image80.jpg











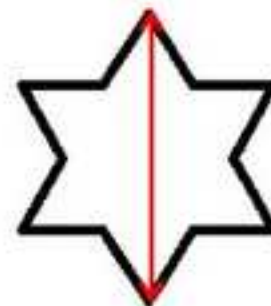
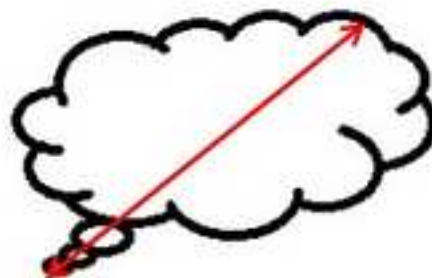
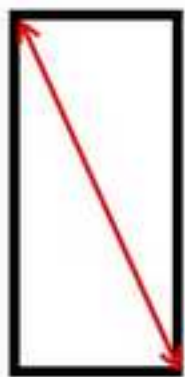
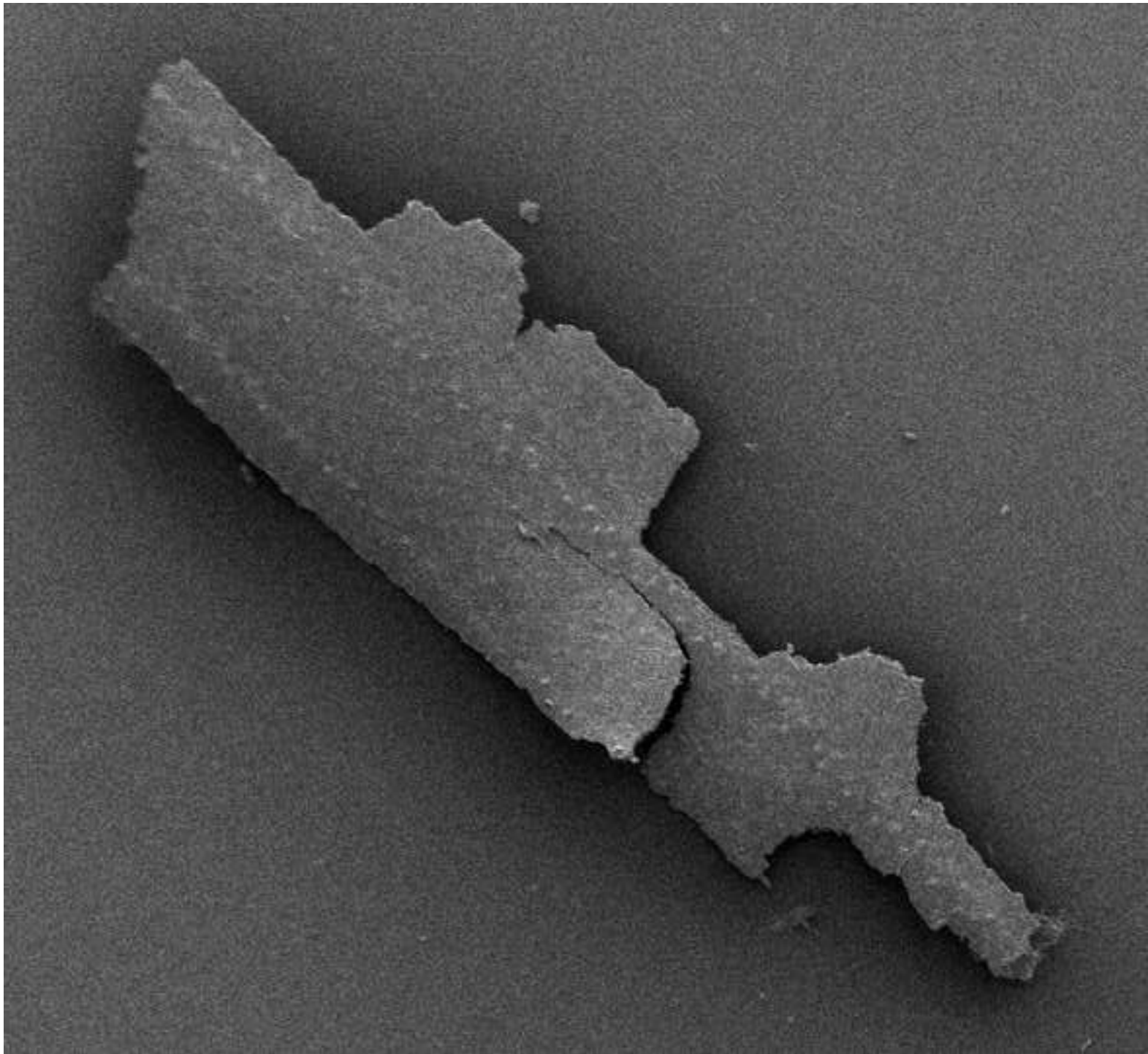
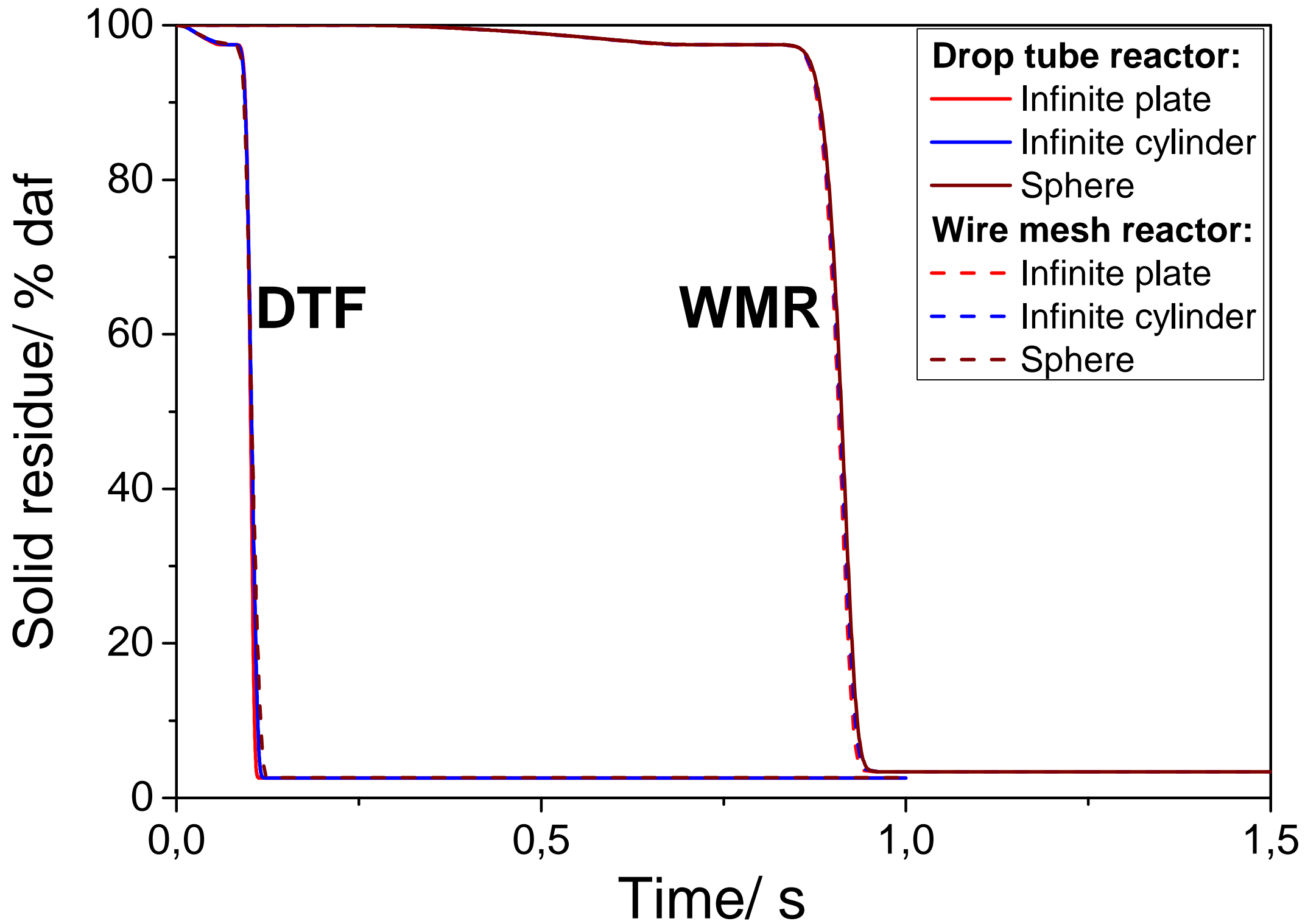
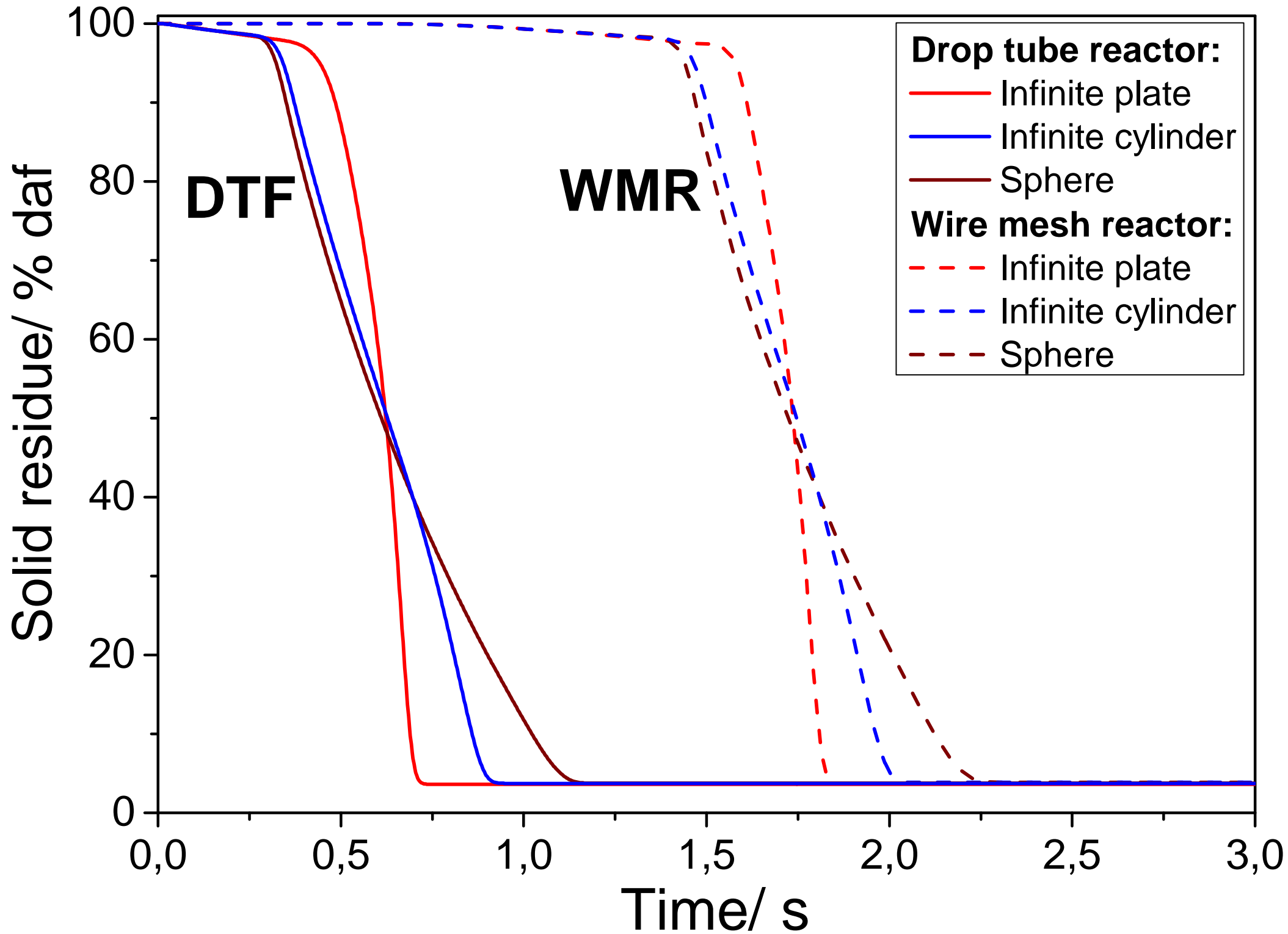


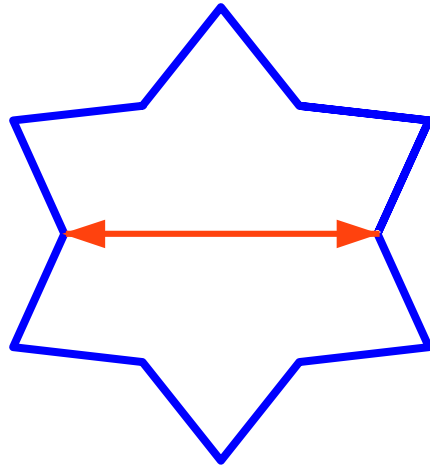
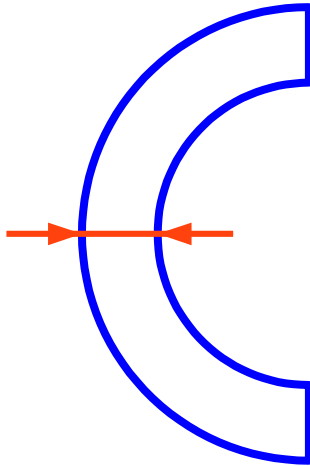
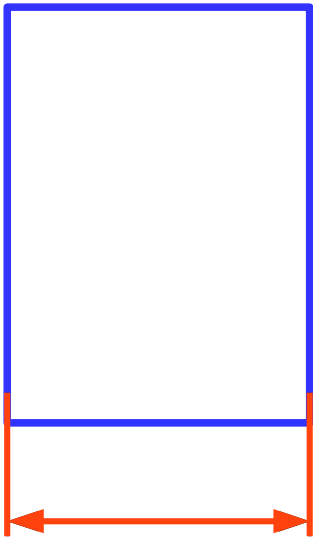
image84.jpg

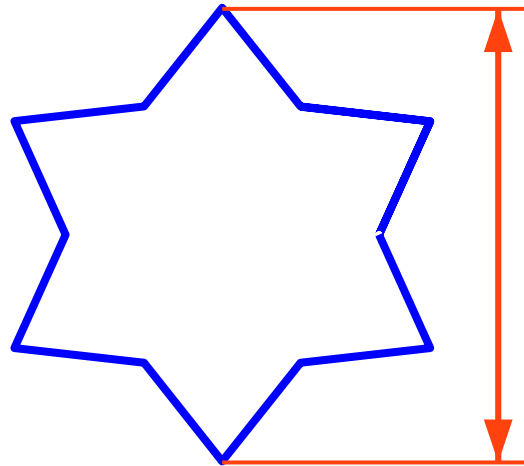
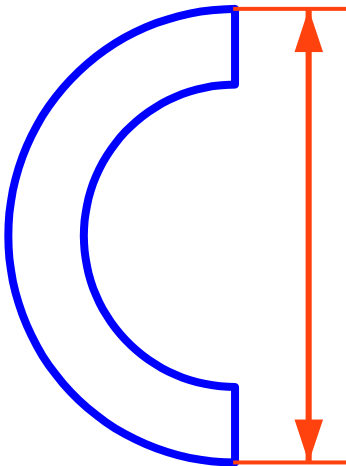
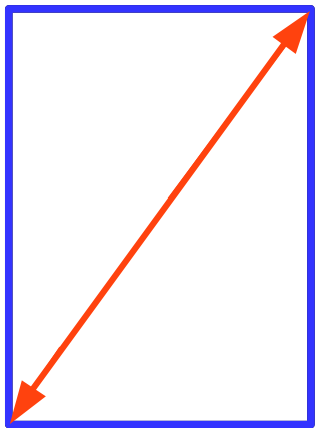
[Click here to download high resolution image](#)

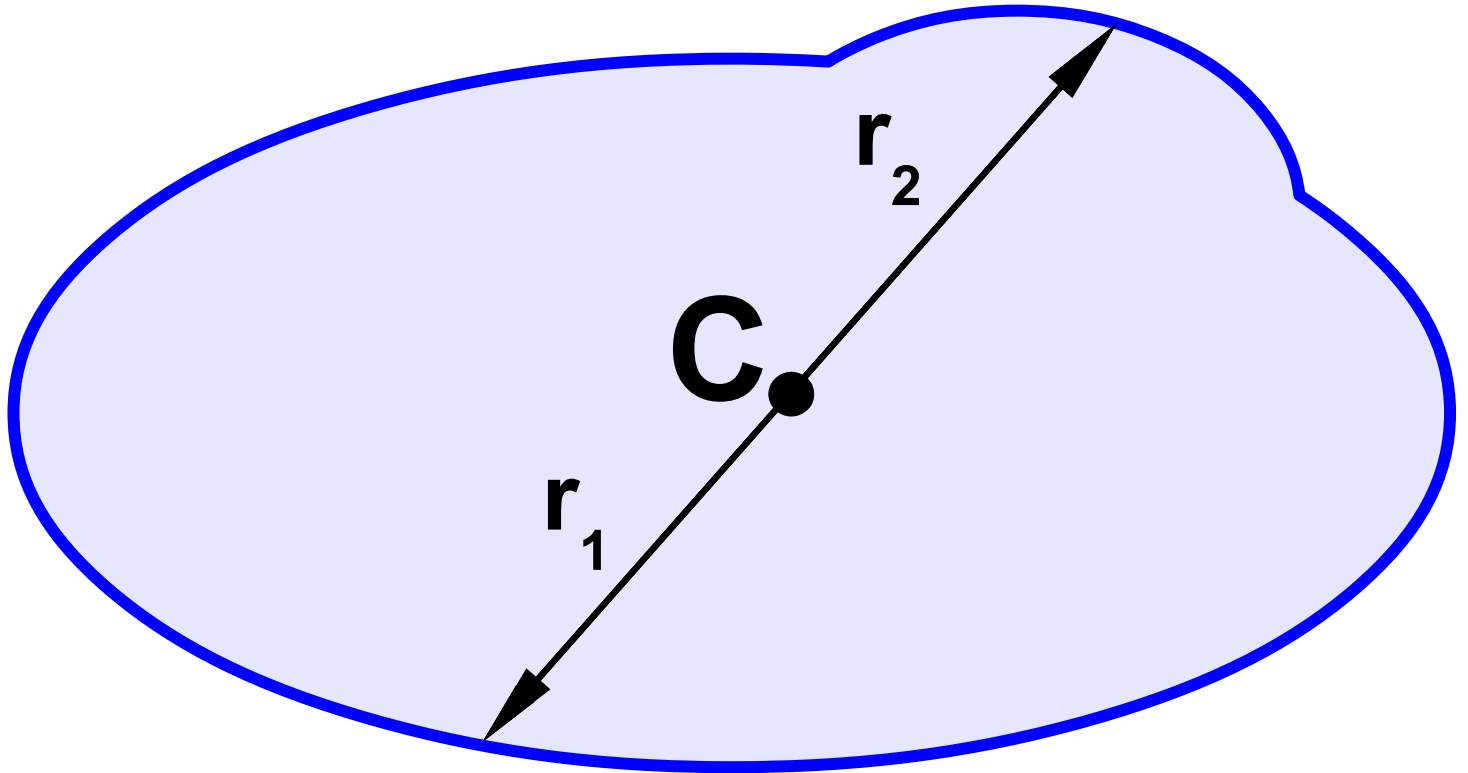


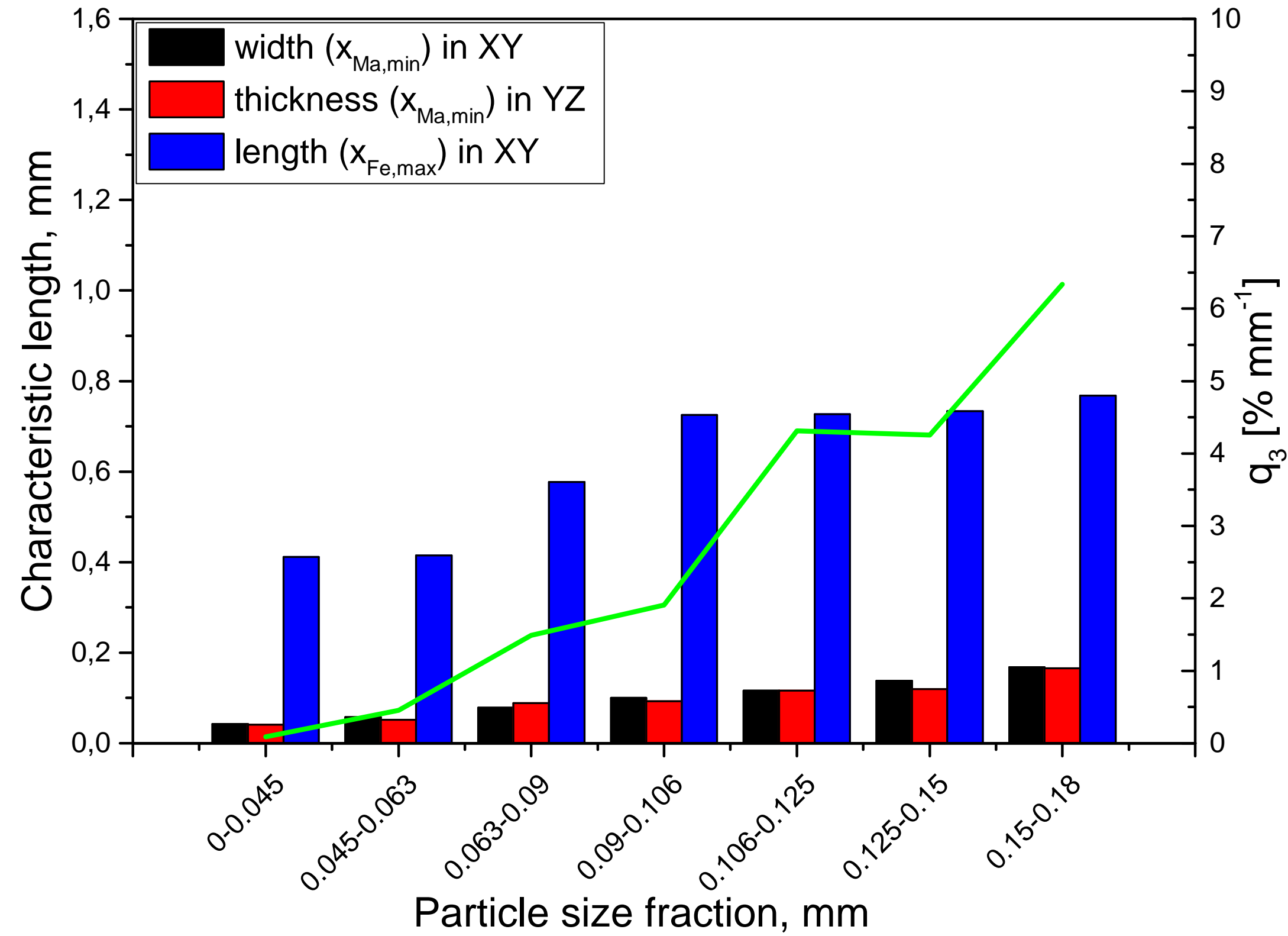


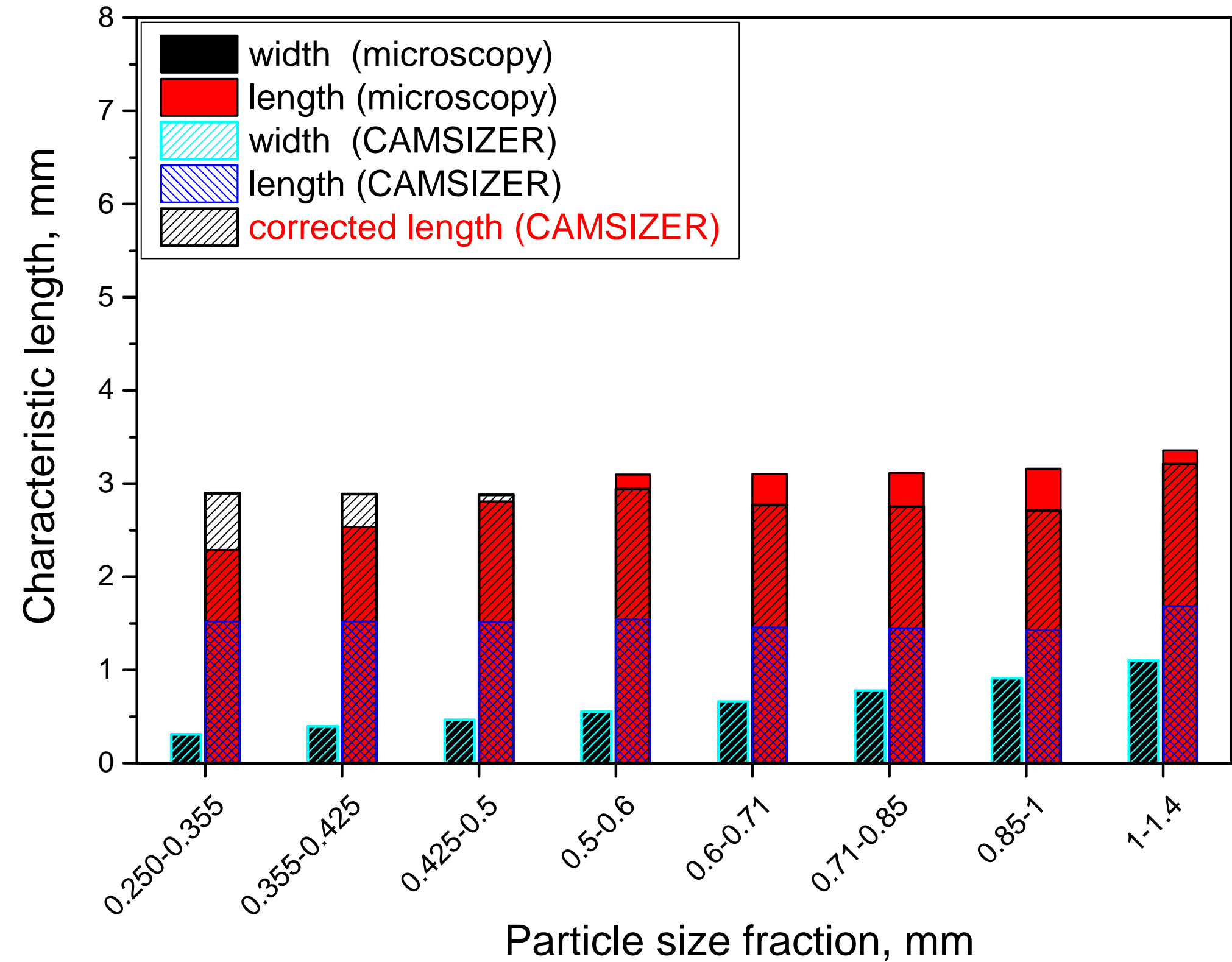


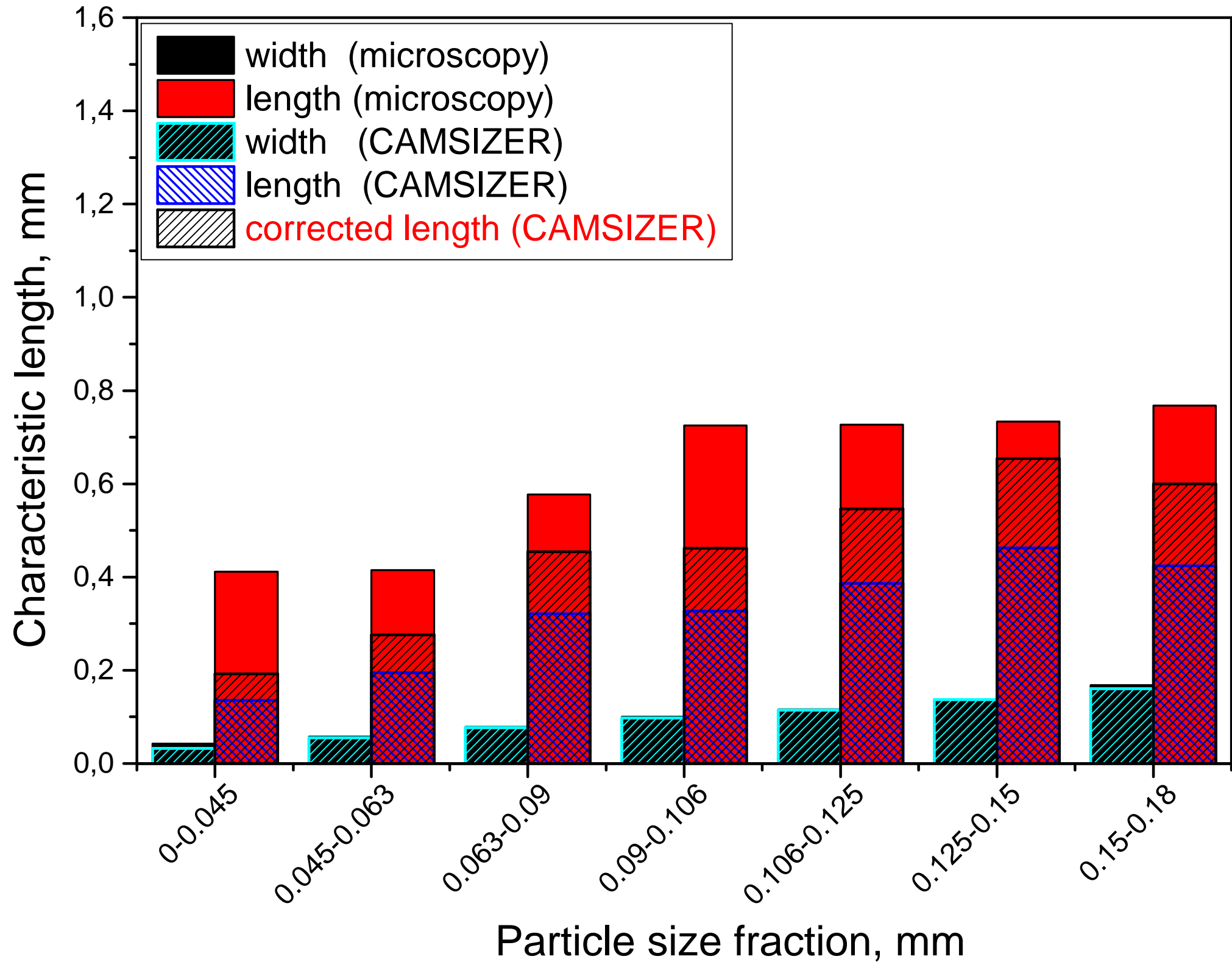


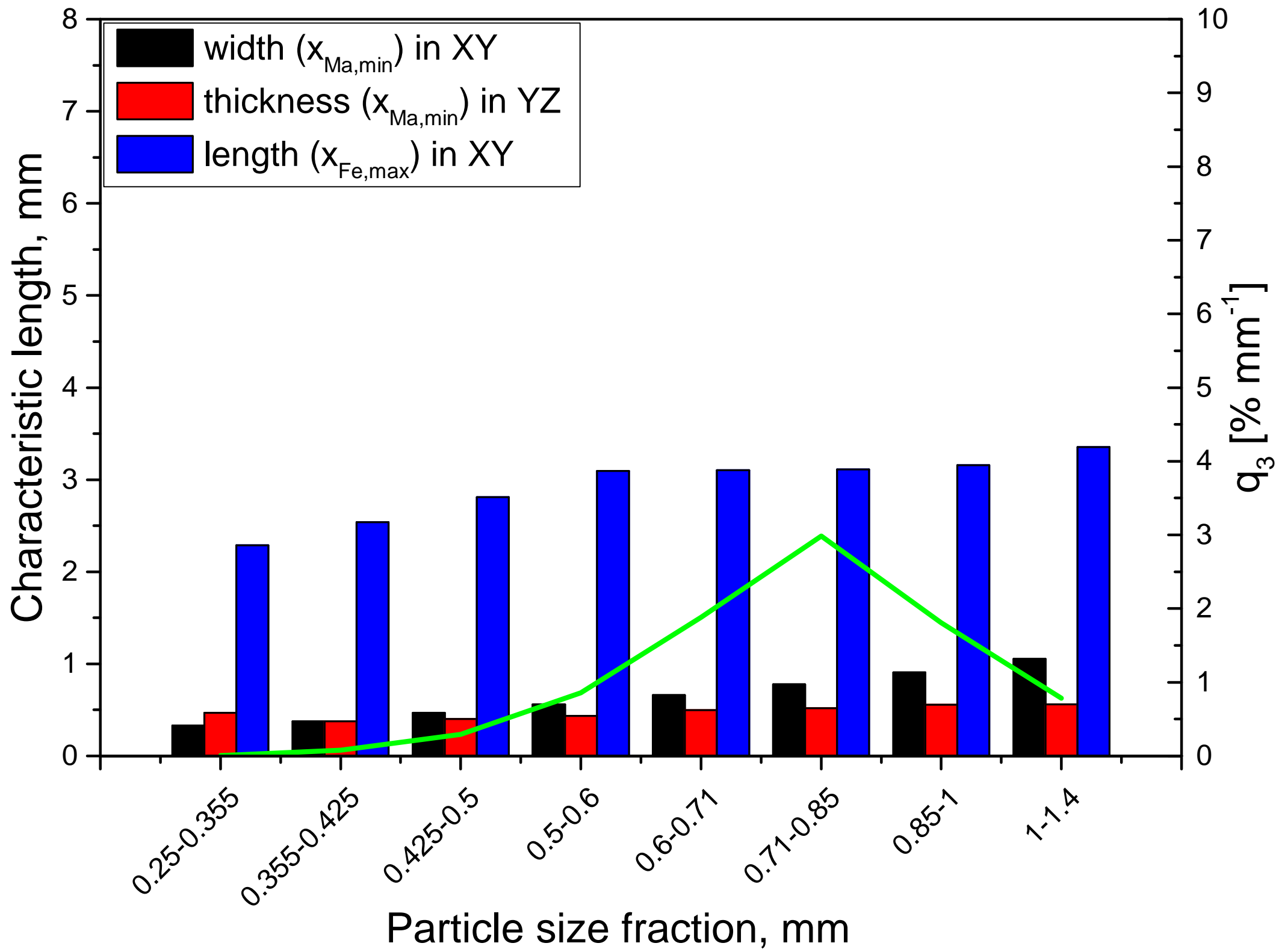


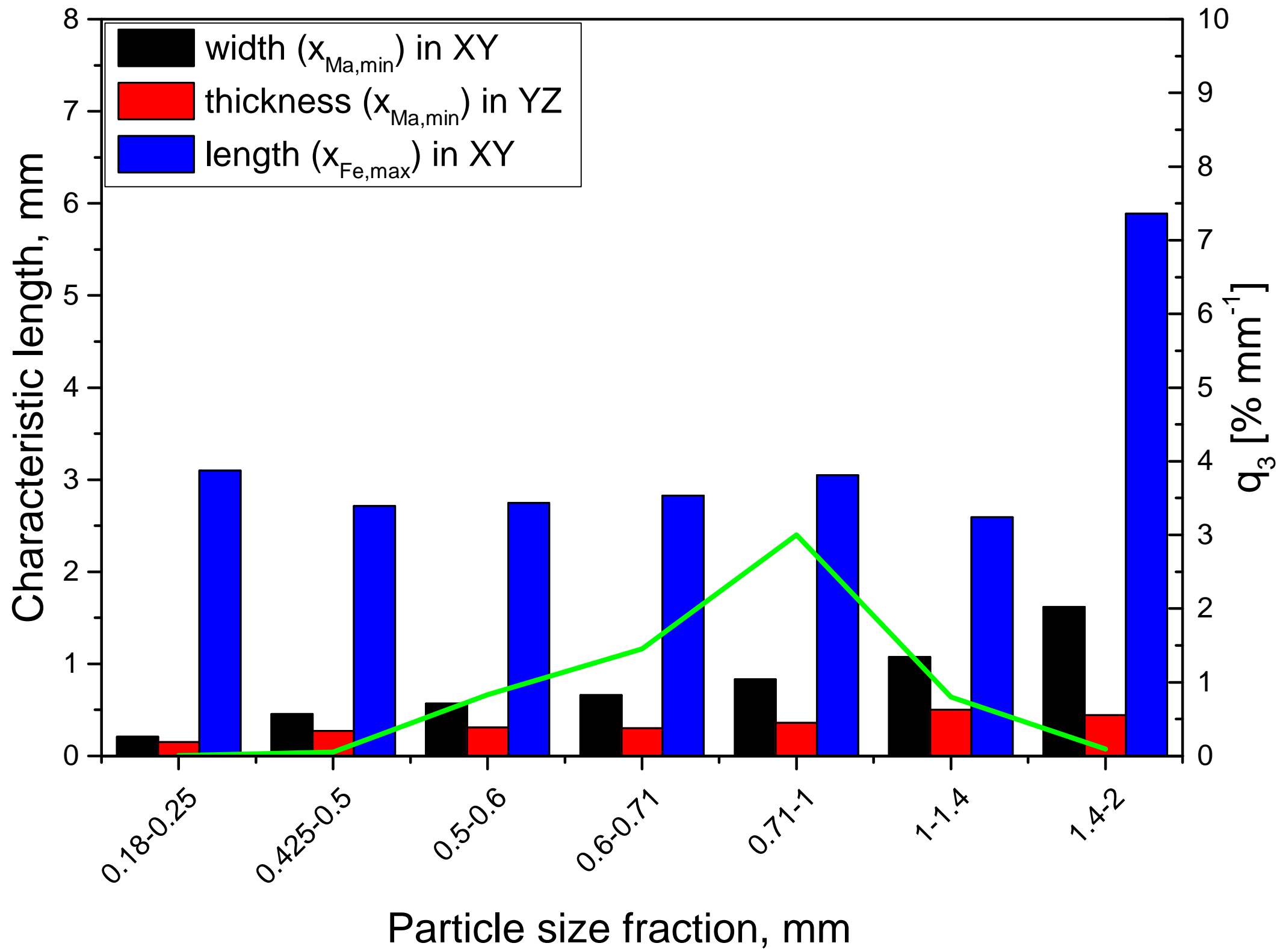


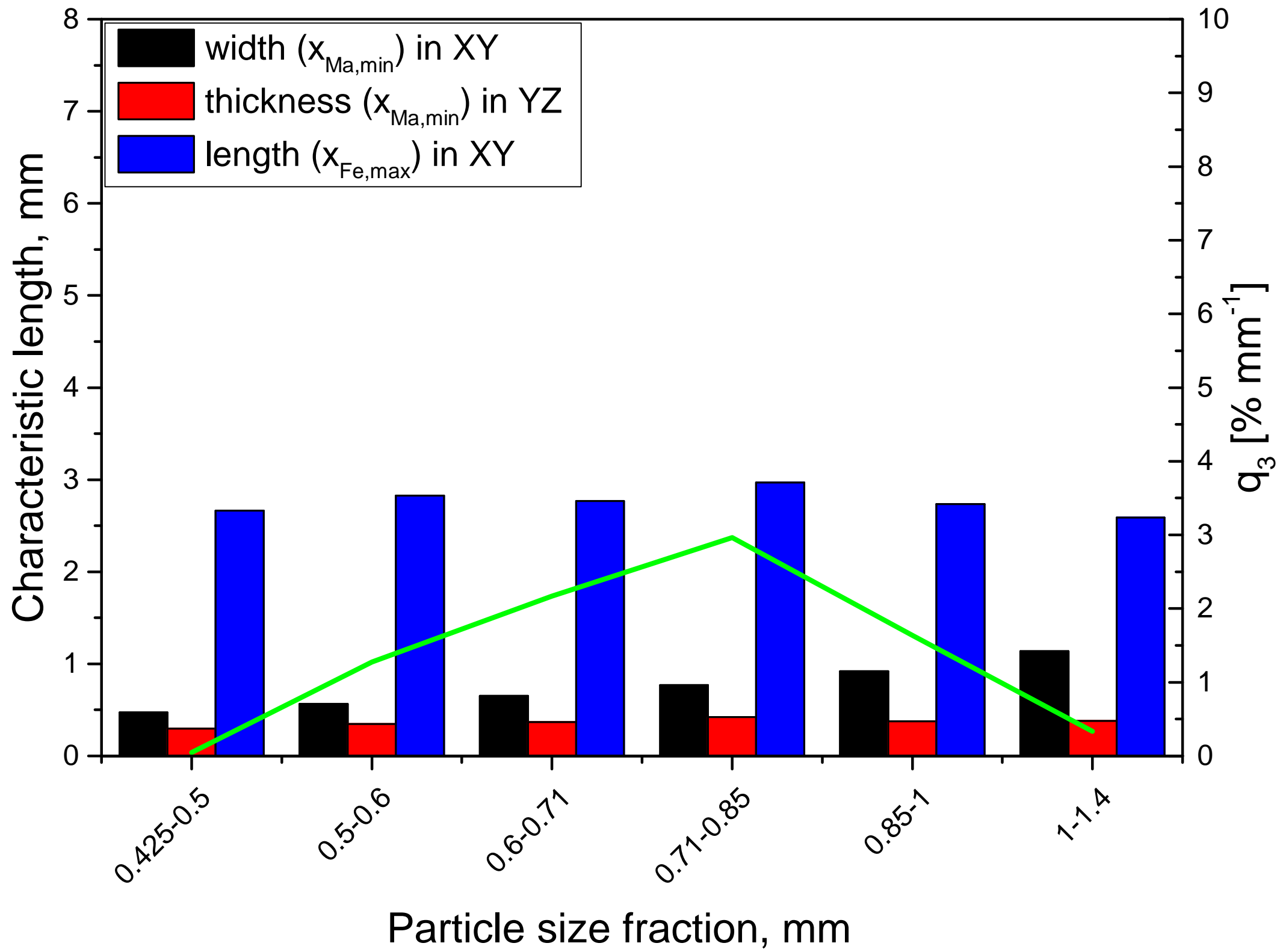












Supplementary Material

[Click here to download Supplementary Material: supplemental_material.pdf](#)

LaTeX Source Files manuscript

[Click here to download LaTeX Source Files: revised_article9.tex](#)

LaTeX Source Files bibtex

[Click here to download LaTeX Source Files: myref9.bib](#)

LaTeX Source Files supplemental material

[Click here to download LaTeX Source Files: supplemental_material.tex](#)